Many-photon effects in time-resolved second harmonic generation from systems in optical cavities

Gopalakrishna, Megha

2024

Many-photon effects in time-resolved second harmonic generation from systems in optical cavities

MEGHA GOPALAKRISHNA
DEPARTMENT OF PHYSICS | FACULTY OF SCIENCE | LUND UNIVERSITY

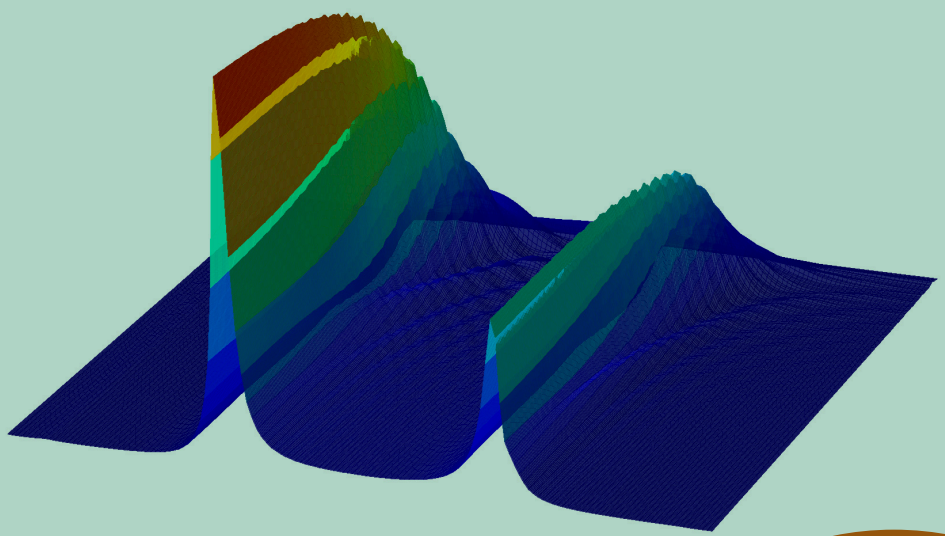

Many-photon effects in time-resolved second harmonic generation from systems in optical cavities.

Many-photon effects in time-resolved second harmonic generation from systems in optical cavities.

by Megha Gopalakrishna

LUND
UNIVERSITY

Thesis for the degree of Doctor of Philosophy
Thesis advisor: Assoc. Prof. Claudio Verdozzi
Faculty opponent: Prof. Göran Johansson

To be presented, with the permission of the Faculty of Science of Lund University, for public criticism in the Rydebrg lecture hall at the Department of Physics on Friday, the 23rd of February 2024 at 13:15.

Organization
LUND UNIVERSITY

Department of Physics
Box 118
SE–221 00 LUND
Sweden

Document name
DOCTORAL DISSERTATION

Date of disputation
2024-02-23

Sponsoring organization

Author(s)
Megha Gopalakrishna

Title and subtitle Many-photon effects in time-resolved second harmonic generation from systems in optical cavities.

Abstract
Second harmonic generation is popular due to its numerous applications in different technologies dealing with multiple fields of science. The rapid technical advancement with the second harmonic generation demands parallel development in the theoretical understanding. With this view in mind, in our three papers, we theoretically investigated second harmonic generation from different systems in an optical cavity, and this thesis is based on these three papers. Our studies are with the cavity, which will confine the photon mode. Also, we can address the low photon regime with the cavity and observe the dominating quantum effects. We analyze the second harmonic generation by observing the fluorescent spectra of the system with time-resolved formalism. In our studies, we also propose a quantum-classical method inspired by the physics of the Caldeira-Leggett model to depict cavity leakage.

In Paper I, we study fluorescent spectra from a Hubbard dimer. As a novelty in the study, along with electron and photon degrees of freedom, we also consider quantum description for nuclear degrees of freedom. With this new description of the Hubbard dimer, we demonstrated a competition between photo-induced dimer dissociation and second harmonic generation.

In Paper II, we investigate the fluorescent spectra of cold boson atoms in an optical lattice and also from a Bose-Einstein condensate. The study outlines the effects of increasing the number of atoms, lattice sites, and the atom-atom interaction on second harmonic generation.

In Paper III, we explore the non-equilibrium Green function method as an alternative to investigate second harmonic generation from a larger Dicke system. In the study, we observe the effect of disorder and electron interaction on second harmonic generation.

Key words
cavity optics, second harmonic generation, Caldeira-Leggett model, cold atoms, optical lattice, Dicke model, electron-photon interaction, exact diagonalization, GKBA

Classification system and/or index terms (if any)

Supplementary bibliographical information

Language
English

ISSN and key title

ISBN
978-91-8039-783-4(print)
978-91-8039-784-1(pdf)

Recipient's notes

Number of pages
123

Price

Security classification

Signature

Date 2024-01-15

Many-photon effects in time-resolved second harmonic generation from systems in optical cavities.

by Megha Gopalakrishna

LUND
UNIVERSITY

A doctoral thesis at a university in Sweden takes either the form of a single, cohesive research study (monograph) or a summary of research papers (compilation thesis), which the doctoral student has written alone or together with one or several other author(s).

In the latter case the thesis consists of two parts. An introductory text puts the research work into context and summarizes the main points of the papers. Then, the research publications themselves are reproduced, together with a description of the individual contributions of the authors. The research papers may either have been already published or are manuscripts at various stages (in press, submitted, or in draft).

Cover illustration front: Second harmonic generation spectrum (adapted from Paper III)

Funding information: Financial support by The Swedish Research Council (VR).

Faculty of Science, Department of Physics

ISBN: 978-91-8039-783-4 (print)
ISBN: 978-91-8039-784-1 (pdf)

Printed in Sweden by Media-Tryck, Lund University, Lund 2024

Dedicated to my Mother and Father

Contents

List of publications

This thesis is based on the following publications, referred to by their Roman numerals:

I **Photon pumping, photodissociation and dissipation at interplay for the fluorescence of a molecule in a cavity**
M. Gopalakrishna, E. Viñas Boström, C. Verdozzi
SciPost Phys. 15, 138 (2023)

We introduced a model to demonstrate a competition between the photo-induced dissociation and second harmonic generation from a Hubbard dimer. Along with the dimer dissociation, we observed a decrease in the intensity of the fluorescent spectra with electron interaction and quenching of second harmonic generation from the slow driving of photons. We also considered cavity leakage in the model and observed a reduction in the intensity of fluorescent spectra.
contribution: I adapted an existing exact diagonalization (ED) code to calculate steady-state second harmonic generations (SHG), and I extended the approach in a time dependent code by implementing the effect of cavity leakage on SHG. I further added all the other necessary extensions to the code. I performed all the calculations, including all the benchmarks necessary during the code development. I analyzed the results under the co-authors' guidance and I wrote the first draft (including the all the figures) and participated actively in writing the final version of the paper.

II **Second harmonic generation from ultracold bosons in an optical cavity**
M. Gopalakrishna, E. Viñas Boström, C. Verdozzi
Submitted, arXiv:2401.05929

This paper studies the second harmonic generation from cold boson atoms. We consider cold atoms in an optical lattice and atoms as a Bose-Einstein condensate in the study. For the optical lattice, with the low atom-atom interaction, increasing the number of atoms increased the intensity of the spectra. However, with strong atom-atom interaction, we observed a reduction in the emission intensity when there are more atoms than the number of lattice sites. In the Bose-Einstein condensate, we observed a trend of identical spectra with increased atoms for low cavity coupling, but the spectrum deviated slightly with the stronger cavity coupling.

contribution: Starting from the computational platform of the first project, I implemented the Hamiltonian for boson ultracold lattices and to discuss the situation of Bose-Einstein condensates. I further added all the other necessary extensions to the code. I performed all the calculations, made all the figures, and provided a first analysis of the results. I wrote the first draft of the paper, and I participated actively in writing the final version of the paper.

III **Time resolved optical response of the Dicke's model via nonequilibrium Green's function approach**
M. Gopalakrishna, Y. Pavlyukh, C. Verdozzi
Submitted, arXiv:2312.13874

We investigated the second harmonic generation from the Dicke model with NEGF formalism. The method was based on the time linear technique and was more efficient than the usual NEGF-GKBA formalism of quadratic scaling. With the NEGF formalism, we could observe fluorescent spectra of SHG for the reasonably large system in the presence of disorder and interaction, which is impossible with ED. We observed that both disorder and electron interaction reduced the intensity of SHG.
contribution: I wrote all the codes necessary for the ED treatment in the presence of interactions and disorder, and I did all the calculations for both the ED and NEGF-GKBA approach. I fully analyzed the ED results and, under the co-authors' guidance, I analyzed the NEGF-GKBA results. I wrote the first draft of the paper (including all the figures), and participated actively in writing the final version of the paper.

All papers are reproduced with permission of their respective publishers.

Acknowledgements

I appreciate the help that I got from every person during my PhD. With your kindness, I'm approaching the end of this fascinating journey. I want to express my gratitude to everyone, especially those mentioned here.

First of all, a big thanks to my supervisor, Claudio Verdozzi, for giving me an opportunity to work with him. With very interesting topics, you introduced me to a fascinating field of quantum optics. You always inspire me with your passion and dedication to science. I have always admired your approach to finding more than one way of doing things. You were kind to me in explaining things, always clarified my doubts, and made me understand multiple concepts. I appreciate that you allowed me to disturb you with small and big questions, even at odd times. Also, I'm very thankful for the care and concern I got from you during the COVID time. I enjoyed working with you and will miss your stories and jokes.

I would like to thank Emil Viñas Boström for collaborating with me on the fascinating projects. You allowed me to approach you many times with big and small questions and helped me understand multiple concepts. In the same breath, I would like to extend my gratitude to Yaroslav Pavlyukh. I enjoyed working and also discussing with you. You were always kind to answer all my questions. I am very grateful to you for the pedagogical Zoom sessions we had.

I want to thank my co-supervisors, Ferdi Aryasetiawan, Marcus Dahlström, and Mathieu Gisselbrecht, for your help and kindness. Many thanks to my office mates Jimmy Ljungberg, Drilon Zenelaj, Stefanos Carlström, Malte Schubert, Mikael Nilsson Tengstrand, Josef Josefi, and Patrick Potts for always maintaining the pleasant working atmosphere in the office. Zhen Zhao, Ayan Pal, and Emil Östberg, I had a fun time with you during the conference, and also thank you for all the scientific discussions. I also want to extend my gratitude to Peter Samuelsson, Andreas Wacker, Andrea Idini, Erik van Loon, Gillis Carlsson, Stephanie Reimann, Jakob Bengtsson, Tomas Brage, and Armin Tavakoli

for always being kind and introducing new and interesting science topics to me through seminars and discussions.

A special thanks to Katarina Lindqvist for being reliable always with the administrative work and taking care of my diet. Thanks to all the emeriti in the division. Cecilia Jarlskog, I enjoyed discussing scientific and non-scientific topics with you. Therese Stridh, thank you for all the help with the administration. I'm sincerely grateful for each and every person at the Mathematical Physics division. I learned a lot from you and had fun during lunch, fika, and the division day.

I want to extend my gratitude to Kartick Tarafder; you always inspire your students to pursue science. I had lots of memorable times with Heena, Kumkum, Om, Smitha, Nitin, Nitish, Rashi, Arvind, Carina, Shatabdi, Abhishek, Somnath, and many more also thank you for the fun potlucks. Manuel, Pavan, and Anchitha, I got lots of help from you during the early days, and I'm very grateful for that. I also would like to thank my extended family and friends back home for all the help and support.

Lastly, I'm grateful to my parents for their unconditional support and love. You are the pillar of my life and education. Thank you for standing by my side in all the decisions I make.

Popular summary

Humans have always been interested in exploring light. The branch of science that studies the nature of light is known as 'optics'. In optics, light is expressed as a ray or as a wave. The description of 'rays' helps explain the phenomena such as reflection and refraction. However, processes such as diffraction and interference, where one observes high and low-intensity patterns, require 'wave' description of light. All these phenomena and descriptions support the wave nature of light. But then processes like 'Black body radiation' and 'photoelectric effect' are explained by considering that light is made up of particles of discrete energy called 'photons'. Hence, light is considered to have a wave-particle duality since it behaves both as a wave and a stream of particles. In this thesis, we consider light confined in a cavity, and hence, we depend on the photon nature of light.

Light plays an essential role in everyday life. It is because of light that we see the world around us. However, in today's tech-driven world, applications of light are far more numerous, communication has become faster, producing energy has become environmental friendly with solar cells, and there are multiple medical applications such as treating cancer. The basic phenomenon that all these applications exploit is the interaction between light and matter.

Light interacting with the matter might interact weakly and cause no effect on the material. However, the discovery of laser made possible to address high-intensity phenomena. Light brings drastic changes to the system in the presence of high intensity sources such as laser. In certain materials, such as 'quartz', the high intensity fields can bring so-called 'non-linear polarization'. The non-linearity of the polarization allowed for multiple applications such as parametric amplification, parametric oscillation, and the frequency conversion of the incident field. Frequency conversion helps achieve sum frequency conversion, difference frequency conversion, and 'high-harmonic generation'. In this thesis, we focus on 'second harmonic generation', in which the frequency of the incident field is doubled.

Theoretically, there are multiple methods that have been considered to investigate second harmonic generation. In this thesis, we work with two of these methods. Also, we investigate second harmonic generation in different systems, and characterize some general trends in the time dependent and steady state spectra.

Part I

Background and Methods

Chapter 1

Introduction

Light falling on a material might or might not get absorbed. If a material absorbs the light, then again, it might or might not emit the absorbed light. Light emitted may or may not be the same as the incident light. Because of all these possibilities, the interaction between light and matter lies at the heart of many revolutionary technologies, such as spectroscopy, laser, microscopy, solar cells, sensors, and many more. One such revolution is second harmonic generation (SHG), where two incident photons on a material result in a single photon with twice the incident frequency. SHG is a non-linear effect requiring an intense light source for observation. Hence, it was first observed only after the discovery of the laser.

Nowadays, SHG is used in a wide range of applications, such as microscopy, biological sensing, short pulse measurement, and characterizing crystals. Even though there has been vast growth in the applications of SHG some aspects in the theoretical understanding of this process are still not fully understood. In this regard, we studied SHG from different systems inside an optical cavity. For the study, we consider the approach of theoretical models. With the models, one may not be able to address the physics associated with a specific system, but it helps gather general trends associated with the physical process.

We consider systems inside an optical cavity because the cavity will confine the electromagnetic mode. When an atom interacts with a laser field in free space, there are a large number of photons that will interact with the atom. However, these photons will interact very weakly with the atom since they will engage with the atom for a short time. But, within a cavity, the cavity photons will have an increased interaction time due to confinement [1]. Also, with the cavity,

one can address the low photon limit in which quantum effects will dominate.

One can study the generation of second harmonics by observing the emission spectra. In our cases, we assume that the photon-induced transitions will conserve the spin. Hence, we refer to the emissions spectra as fluorescent spectra and study time-resolved fluorescent spectra. SHG can be investigated by observing steady-state fluorescent spectra. However, monitoring the emissions spectra throughout time helps understand and analyze the inherent physical processes.

The methods used in our studies are exact diagonalization and nonequilibrium Green functions. Exact diagonalization refers to solving the Schrödinger equation exactly. As the system gets larger, obtaining the exact result could be computationally demanding and impractical in most cases. However, for a reasonably "small" system, the solutions of exact diagonalization stand as a benchmark and can also be used to verify other methods that involve assumption and/or approximations. The nonequilibrium Green function method is well known in studying time dynamics. It is also computationally expensive, but with the generalized Kadanoff-Baym ansatz, one can transform the quadratic time-evolving framework to a single time scheme. Then, the computational time will be reduced drastically. Hence, though the exact diagonalization is an exact method, the Green function gets an edge over it, and some studies that are impossible to carry out with the exact diagonalization become viable with the Green function approach.

To summarize the context of this thesis, In Paper I, we studied competition between dimer dissociation and the generation of second harmonic. The electron's degrees of freedom, dimer nuclear degrees of freedom, and photon fields are all treated quantum mechanically. In this study, we also depicted photon leakage from the cavity via coupling baths of the classical oscillators to the photon fields. In Paper II, we studied SHG from cold bosonic atoms in an optical lattice and from a boson atom condensate. In this study, we explored the effects of atom-atom interaction on the fluorescent spectra. Both of the studies were carried out with exact diagonalization. As said earlier, the ED method becomes impractical for larger systems. In Paper III, we investigated the generation of second harmonics from the Dicke model using the nonequilibrium Green function method. Hence, we considered a reasonably larger Dicke system, and in the study, we observed the effect of disorder and electron interaction on SHG.

Now, we will outline the structure of this thesis. In the second chapter, we briefly describe the numerical methods used in the papers. The following three chapters in Part I contain an overview of the paper's contents. The sixth chapter includes

a summary and an outlook for further research. We hope Part I will acquaint the readers with the necessary materials to read papers in Part II.

Chapter 2

Theoretical and computational methods

2.1 Exact Diagonalization

In quantum mechanics, the wave function obtained by solving the Schrödinger equation contains all the information about the system. By representing the Hamiltonian of the system in a matrix form, solutions to the Schrödinger equation are obtained by diagonalizing the matrix. This method is known as exact diagonalization (ED). Of course, when the system becomes larger, ED becomes impractical. But sometimes, in theoretical studies, smaller systems can be used to gather insight in to more complex system, and ED becomes a prominent tool to explore such systems.

The dynamics of a quantum system is understood by observing the time evolution of the wave function of the system. The time-evolved state of the system is obtained by acting with the time evolution operator on the system's initial state. When the Hamiltonian H is time-independent, the time evolution of the initial state $|\psi(0)\rangle$ is given by,

$$|\psi(t)\rangle = e^{-\mathrm{i}Ht}|\psi(0)\rangle \tag{2.1}$$

In all the discussions we consider $\hbar = 1$.

With the set of eigenfunctions λ of H, the time evolution will be re-represented as,

$$|\psi(t)\rangle = \sum_{\lambda} e^{-\mathrm{i}E_\lambda t}|\lambda\rangle\langle\lambda|\psi(0)\rangle \tag{2.2}$$

This method of time evolution is not applicable when the Hamiltonian is time-dependent. In that case, we consider time evolution in small-time steps Δ. With eigenvalues E_λ corresponding to time $t + \Delta/2$ the time evolution will be as follows,

$$|\psi(t+\Delta)\rangle \approx \sum_\lambda e^{-\mathrm{i}E_\lambda \Delta} |\lambda\rangle\langle\lambda|\psi(t)\rangle \tag{2.3}$$

In the above equation Δ is assumed small enough that $\int_t^{t+\Delta} H(t')dt' \approx H(t+\frac{\Delta}{2})\Delta$. The method of ED solves the Hamiltonian exactly without any assumptions. But, since the Hilbert space scales unfavourably with enlarging the physical system, soon with the increased system size ED becomes practically impossible [2, 3, 4]. Hence, ED is preferred for smaller systems and can be considered as a benchmark for other methods used in more complicated studies.

2.2 Lanczos algorithm

The problem with a growing Hilbert space met by ED can be compensated at some extent by performing the time evolution via the Lanczos algorithm [5, 2, 3, 4, 6]. With the Lanczos algorithm, instead of diagonalizing the full Hamiltonian H, a smaller tridiagonal Hamiltonian H_L is constructed, which comes from approximating the full $e^{-iH(t+\frac{\Delta}{2})\Delta}$ in an optmized basis $|V_k\rangle$, with $k \leq N_\kappa$ and N_κ small (as shown below, the vectors $\{V_k\}$ are related to the application of $[e^{-iH(t+\frac{\Delta}{2})\Delta}]^k$ to $|\Psi(t)\rangle$. The time evolution $\Psi(t) \to \Psi(t+\Delta)$ is then obtained with a suitable modification of Eq. 2.3 projected in the $\{V_k\}$ space. Since $N_\kappa \equiv \mathrm{Dim}(H_L)$ is chosen greatly smaller than $\mathrm{Dim}(H)$, the time evolution is again possible, after making sure (via a proper choice of Δ and N_κ) that convergence is assured within the $\{V_k\}$ space. For sparse Hamiltonians, with a relatively small number of nonzero matrix elements, the (highly reduced) number of operations to perform matrix-vector multiplications to produce the basis $\{V_k\}$ at each time step is also an important factor increasing the numerical efficiency of the Lanczos algorithm. The latter is thus especially suitable for large sparse Hamiltonians.

In more detail, the Lanczos algorithm involves span of the orthonormal vectors, also known as Lanczos vectors. They can be obtained by the successive application of H on the system's state (such as $\psi(0)$ for time-independent Hamiltonian). Orthonormalization follows the principle of Gram-Schmidt orthonormalization. The time evolution with the Lanczos algorithm is initialized by the seed state

$|V_0\rangle = \psi(0)$, where $\psi(0)$ is the initial state. Second Lanczos vector $|V_1\rangle$ orthonormal to $|V_0\rangle$ will be,

$$|\tilde{v}_1\rangle = H|V_0\rangle - u_0|V_0\rangle,$$
$$u_0 = \langle V_0|H|V_0\rangle, \quad w_1 = \sqrt{\langle \tilde{v}_1|\tilde{v}_1\rangle},$$
$$|V_1\rangle = \frac{1}{w_1}|\tilde{v}_1\rangle. \tag{2.4}$$

Further, the construction of mth Lanczos vectors is as follows,

$$|\tilde{v}_m\rangle = H|V_{m-1}\rangle - u_{m-1}|V_{m-1}\rangle - w_{m-1}|V_{m-2}\rangle,$$
$$u_{m-1} = \langle V_{m-1}|H|V_{m-1}\rangle, \quad w_{m-1} = \sqrt{\langle \tilde{v}_{m-1}|\tilde{v}_{m-1}\rangle},$$
$$|V_m\rangle = \frac{1}{w_m}|\tilde{v}_m\rangle. \tag{2.5}$$

After observing that increasing the dimension of the Krylov space will not change the results, time evolution is assumed to be converged. For the convergence observed with a maximum Lanczos vector $|V_\kappa\rangle$, the Lanczos basis is $\{|V_0\rangle, |V_1\rangle, |V_2\rangle, ..., |V_\kappa\rangle\}$. As we can observe the Lanczos Hamiltonian H_L is tridiagonal and κ determines the size of H_L.

$$H_L = \begin{pmatrix} u_0 & w_1 & 0 & 0 & 0 & \cdots \\ w_1 & u_1 & w_2 & 0 & 0 & \cdots \\ 0 & w_2 & u_2 & w_3 & 0 & \cdots \\ 0 & 0 & w_3 & u_3 & w_4 & \cdots \\ \vdots & \vdots & \vdots & \vdots & \vdots & \ddots \end{pmatrix} \tag{2.6}$$

With the Lanczos vectors, time evolved state for the time-independent Hamiltonian will be,

$$|\psi(t)\rangle = \sum_{m,\lambda^{(L)}} |V_m\rangle\langle V_m|e^{-\mathrm{i}E_\lambda^{(L)}t}|\lambda^{(L)}\rangle\langle\lambda^{(L)}|V_0\rangle, \tag{2.7}$$

where $E_\lambda^{(L)}$ corresponds to eigenvalues of Lanczos Hamiltonian H_L and $V_0 = \psi(0)$. The Lanczos algorithm will be helpful whenever κ is significantly smaller than the size of the Hilbert space corresponding to actual Hamiltonian H. When the Hamiltonian is time-dependent, time evolution will be considered in steps as in Eq. 2.3. For the time evolved state $\psi(t + \Delta)$, the seed state V_0 will be $\psi(t)$.

2.3 Nonequilibrium Green function for electron-photon interacting systems

As mentioned earlier, in Paper III we explore the scope of NEGF method for studying light-matter coupled system. The correlation based NEGF method can be used to extract the relevant observables as time dependent averages. Some approximations will be adopted with the method to make it less expensive.

2.3.1 NEGF for fermions

This section gives a brief summary of the NEGF method for fermions (electrons). More detailed presentations of the method can be found in [7, 8, 9, 10]

Consider an interacting system in the ground state $|\psi_g\rangle$ at an initial time $t = 0$. The system is described by an Hamiltonian $H(t) = H_0 + V(t) + H_I$, where $H_0, V(t)$ respectively denote the static and time dependent independent-particle contribution (i.e. $V(t)$ describes the external perturbation, which usually starts to act for $t > 0$), and H_I accounts for the electron-electron interaction. The average of an operator $\mathcal{O}$ at time $t > 0$ is given by

$$\langle \mathcal{O}(t) \rangle = \langle \psi_g | \mathcal{U}(0,t)\, \mathcal{O}\, \mathcal{U}(t,0) | \psi_g \rangle, \tag{2.8}$$

where $\mathcal{U}(t'', t')$ is a time evolution operator from time t' to t'', and $\mathcal{U}(t,0)^\dagger = \mathcal{U}(0,t)$ is a property of the time evolution operator. One formulation of the NEGF approach expands on the viewpoint of Eq. 2.8, using as starting point the fully interacting system at $t = 0$. Much work with NEGF has been and is done along these lines. However, in several recent treatments and actual numerical implementations, another prescription is followed in practice, which rests i) on an artificial adiabatic switching approach of the interactions starting from an noninteracting system in the remote past, and ii) the assumption that in this way one reaches the ground state of the interacting system, to then start the actual nonequilibrium dynamics of interest. Our brief introduction here to NEGF will be based on the adiabatic approach (see e.g [7] for an extended discussion). Accordingly, for the adiabatic switch-on Hamiltonian one considers

$$H_\sigma(t) = H_0 + e^{-\sigma|t|} H_I, \tag{2.9}$$

and, for the Gell-Mann-Low theorem, $|\phi(0)\rangle \equiv \mathcal{U}_\sigma(0, -\infty)|\phi_g\rangle$, (where $|\phi_g\rangle$ is the non-interacting ground state in the remote past, i.e. of H_0) is an eigenstate of $H_\sigma(0) \equiv H_0 + H_I$. The adiabatic connection is then realized if $|\phi(0)\rangle = |\psi_g\rangle$.

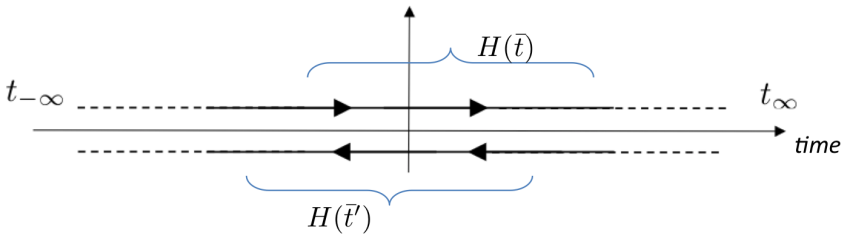

Figure 2.1: The contour $\mathbb{C}$ introduced in Eq. 2.12. The time argument of H on the two branches of $\mathbb{C}$ is according to Eq. 2.11. The specification of H at positive and negative times, is given in the main text. The figure is adapted from [7]

Within the adiabatic approach, Eq. 2.8 is rewritten as

$$\langle \mathcal{O}(t) \rangle = \langle \phi_g | \mathcal{U}_\sigma(-\infty, 0) \mathcal{U}(0, t)\, \mathcal{O}\, \mathcal{U}(t, 0) \mathcal{U}_\sigma(0, -\infty) | \phi_g \rangle, \tag{2.10}$$

This expression can be compacted by extending the definition of $H(t)$ at negative times as $H(t < 0) \equiv H_\sigma(t)$, and using the time ordering ($\mathcal{T}$) and the anti-time ordering ($\bar{\mathcal{T}}$) operators (specified below):

$$\langle \mathcal{O}(t) \rangle = \langle \phi_g | \bar{\mathcal{T}}(e^{-\mathrm{i} \int_t^{-\infty} d\bar{t}'\, H(\bar{t}')})\, \mathcal{O}\, \mathcal{T}(e^{-\mathrm{i} \int_{-\infty}^{t} d\bar{t}\, H(\bar{t})}) | \phi_g \rangle. \tag{2.11}$$

Here, $\mathcal{T}$ and $\bar{\mathcal{T}}$ order operators within the brackets. Specifically, $\mathcal{T}$ orders operators with later time to left, whereas $\bar{\mathcal{T}}$ will order later time operators to the right. The ordering of times guided by $\mathcal{T}$ and $\bar{\mathcal{T}}$ can be combined in an oriented contour $\mathbb{C}$ shown in Fig. 2.1.

The notion of contour is a core element of NEGF theory; it was pioneered by Schwinger [11], reconsidered by Keldysh [12] and also by Konstantinov and Perel' [13] and Danielewicz [14]. It can be applied in different forms and to different situations. Here we focus on the contour for the adiabatic approach as shown in Fig. 2.1. Introducing an orientation on $\mathbb{C}$, the average $\langle \mathcal{O}(t) \rangle$ can finally be expressed as

$$\langle \mathcal{O}(t) \rangle = \langle \phi_g | \mathcal{T}_\mathbb{C} \{ e^{-\mathrm{i} \int_\mathbb{C} d\bar{\tau}\, H(\bar{\tau})} \mathcal{O}(\tau) \} | \phi_g \rangle, \tag{2.12}$$

where τ represents the contour time used to specify the real time t placed on the forward or the backward branch of the contour.

Single particle Green function

The contour Green function is a fundamental part of NEGF, and the one particle contour Green function is given by,

$$G_{ij}(\tau,\tau') = \frac{1}{\mathrm{i}}\langle\phi_g|\mathcal{T}_{\mathbb{C}}\{e^{-\mathrm{i}\int_{\mathbb{C}} d\bar{z}\, H(\bar{z})}\hat{a}_i(\tau)\hat{a}_j^\dagger(\tau')\}|\phi_g\rangle, \tag{2.13}$$

where $\hat{a}_i$ annihilates an electron at state i. Here i represents both the orbital and spin labels. The fermionic operators $\hat{a}_i$ and $\hat{a}_j$ follow standard anti-commutation relations, hence the Green function will change sign if τ' is later than τ.

Even though $t > t'$, τ' could be later than τ depending on placement of τ and τ' on the contour. If τ' is later than τ then,

$$G_{ij}^{<}(t,t') = -\frac{1}{\mathrm{i}}\langle\phi_g|\mathcal{U}(-\infty,t')\,\hat{a}_j^\dagger\,\mathcal{U}(t',t)\,\hat{a}_i\,\mathcal{U}(t,-\infty)|\phi_g\rangle. \tag{2.14}$$

When τ is later than τ',

$$G_{ij}^{>}(t,t') = \frac{1}{\mathrm{i}}\langle\phi_g|\mathcal{U}(-\infty,t)\,\hat{a}_i\,\mathcal{U}(t,t')\,\hat{a}_j^\dagger\,\mathcal{U}(t',-\infty)|\phi_g\rangle. \tag{2.15}$$

The contour Green function can be rewritten with the lesser and greater Green functions as

$$G_{ij}(\tau,\tau') = \Theta(\tau,\tau')G_{ij}^{>}(t,t') + \Theta(\tau',\tau)G_{ij}^{<}(t,t'), \tag{2.16}$$

where $\Theta(\tau,\tau')$ is a step function which becomes 1 when τ is later than τ' and 0 when τ is earlier than τ'.

The equal-time lesser Green function corresponds to the density matrix; that is, $G_{ij}^{<}(t,t) = \mathrm{i}\rho_{ij}^{<}(t)$ (the reason for using the superscript "$<$" in ρ will become clear later on). Hence time dependent average of an observable can be evaluated as

$$\langle\mathcal{O}(t)\rangle = \sum_{ij}\mathcal{O}_{ij}\rho_{ji}^{<}(t) = -\mathrm{i}\sum_{ij}\mathcal{O}_{ij}G_{ji}^{<}(t,t). \tag{2.17}$$

Dyson equation

In the presence of electron-electron interactions, the one particle Green function G can be expressed in terms of the non-interacting Green function G_0, and a quantity Σ known as the self energy. The complex behavior of the system due

to the interactions is thus incorporated in Σ. With the introduction of Σ, the one particle Green function can be obtained from the Dyson equation

$$G(\tau,\tau') = G_0(\tau,\tau') + \int_{\mathbb{C}} d\tau_1 d\tau_2 G_0(\tau,\tau_1)\Sigma(\tau_1,\tau_2)G(\tau_2,\tau'). \tag{2.18}$$

Here G_0 represents the non-interacting Green function.

Generalized Kadanoff-Baym Ansatz

The integro-differential form of the Dyson equation is

$$\left(\mathrm{i}\frac{d}{d\tau} - h(t)\right) G(\tau,\tau') = \delta(\tau,\tau') + \int_{\mathbb{C}} d\tau_1 \Sigma(\tau,\tau_1)G(\tau_1,\tau'). \tag{2.19}$$

It describes the time evolution of the Green function and $h(t)$ is a single particle Hamiltonian. For t considered along the forward branch of the contour and t' along the backward branch,

$$\left(\mathrm{i}\frac{d}{dt} - h(t)\right) G^{<}(t,t') = \int_{-\infty}^{\infty} dt_1 \Big(\Sigma^R(t,t_1)G^{<}(t_1,t') + \Sigma^{<}(t,t_1)G^A(t_1,t')\Big). \tag{2.20}$$

When t' is along the forward branch and t along the backward branch,

$$G^{>}(t,t')\left(-\mathrm{i}\frac{\overleftarrow{d}}{dt'} - h(t')\right) = \int_{-\infty}^{\infty} dt_1 \Big(G^R(t,t_1)\Sigma^{>}(t_1,t') + G^{>}(t,t_1)\Sigma^A(t_1,t')\Big). \tag{2.21}$$

Equations 2.20 and 2.21 are known as the Kadanoff-Baym equations. In the equations retarded and advanced component of a correlator function $F(t,\bar{t})$ are defined as

$$F^R(t,\bar{t}) = \Theta(t-\bar{t})\big[F^{>}(t,\bar{t}) - F^{<}(t,\bar{t})\big],$$
$$F^A(t,\bar{t}) = -\Theta(\bar{t}-t)\big[F^{>}(t,\bar{t}) - F^{<}(t,\bar{t})\big].$$

Here $\theta(t-\bar{t})$ is the Heaviside step function which will assume value 1 when $t > \bar{t}$ or else 0 for $t < \bar{t}$.

The cubic scaling of the Kadanoff-Baym equations with time makes the method numerically expensive. Hence Lipavsky *et al.* [15] introduced the so-called Generalized Kadanoff-Baym Ansatz (GKBA), which permits to have a time evolution of NEGF that scales quadratically with time. In GKBA, $G^{<}(t,\bar{t})$ and $G^{>}(t,\bar{t})$

are expressed in terms of the one particle density matrix along with the retarded and advanced propagator as

$$G^{\lessgtr}(t,\bar{t}) = -G^{R}(t,\bar{t})\rho^{\lessgtr}(\bar{t}) + \rho^{\lessgtr}(t)G^{A}(t,\bar{t}), \tag{2.22}$$

where $G^{<}_{ij}(t,t) = \mathrm{i}\rho^{<}_{ij}(t)$ and $G^{>}_{ij}(t,t) = \mathrm{i}\rho^{>}_{ij}(t)$. The function $\rho^{<}_{ij}(t)$ corresponds to the electron density matrix $\rho_{ij}(t)$. The GKBA ansatz in Eq. 2.22 is valid for non-interacting system or in the Hartree-Fock approximation [15, 7]; however, more in general, it represents an approximation to facilitate NEGF calculations.

Using the above equations in the Kadanoff-Baym equations 2.20 and 2.21,

$$\frac{d}{dt}\rho^{<}(t) + \mathrm{i}[h^{HF}(t), \rho^{<}(t)] = -I_e(t) - I_e^{\dagger}(t), \tag{2.23}$$

where $h^{HF}(t)$ is the Hartree-Fock Hamiltonian and $I_e(t)$ is a collision integral defined as

$$I_e(t) = \int_{-\infty}^{\infty} dt_1 \Big(\tilde{\Sigma}^{R}(t,t_1)G^{<}(t_1,t) + \tilde{\Sigma}^{<}(t,t_1)G^{A}(t_1,t) \Big). \tag{2.24}$$

Using the GKBA expression of Eq. 2.22, the lesser and greater Green functions now depend on the one particle density matrix. However, to close the equations, G_R and G_A are needed and usually Hartree-Fock propagators are used for the retarded and advanced components. In the collision integral $I_e(t)$, the self energy $\tilde{\Sigma}$ excludes the Hartree-Fock self energy, $\Sigma = \tilde{\Sigma} + \Sigma^{HF}$. The Hartree-Fock self energy is related to the Hartree-Fock potential through $\Sigma^{HF}(\tau,\tau') = \delta(\tau,\tau')V^{HF}(t)$, and the Hartree-Fock potential depends on one particle density matrix via $V^{HF}_{ij}(t) = \sum_{pq}(v_{ipqj} - v_{ipjq})\rho^{<}_{pq}(t)$. Here v_{ipqj} and v_{ipjq} are components of the Coulomb interaction tensor. Since the Hartree-Fock self energy is a function of the one particle density matrix, it is usually incorporated in the one particle Hamiltonian. Hence, the Hartree-Fock Hamiltonian is defined as $h^{HF}(t) = h(t) + V^{HF}(t)$.

2.3.2 GKBA for interacting electron-photon systems

In Paper III, we studied the fluorescent emission of a series of two-level systems (TLSs) interacting with a cavity field. The system in question is known in the literature as the Dicke model [16], and it has been extensively used to study different aspects of cavity quantum electrodynamics. Explicitly, the model Hamiltonian used in our study is

$$H_D = \sum_{\boldsymbol{i}=1}^{L} w_{\boldsymbol{i}} s^{z}_{\boldsymbol{i}} + \omega_0 b_1^{\dagger}b_1 + \omega b_2^{\dagger}b_2 + [g_{in}(b_1^{\dagger} + b_1) + g_{fl}e^{-\Gamma t}(b_2^{\dagger} + b_2)] \sum_{\boldsymbol{i}=1}^{L} 2s^{x}_{\boldsymbol{i}} + \sum_{<\boldsymbol{i},\boldsymbol{j}>}^{L} \frac{u_e}{2}\tilde{n}^{e}_{\boldsymbol{i}}\tilde{n}^{e}_{\boldsymbol{j}}, \tag{2.25}$$

In Eq. 2.25, $s^j_{\boldsymbol{i}} = \frac{1}{2}\sum_{\tau\tau'} d^\dagger_{\tau,\boldsymbol{i}}\sigma^j_{\tau\tau'}d_{\tau',\boldsymbol{i}}$ are the spin operators, σ^j are the Pauli spin matrices ($j = x, y, z$), $\tau = 1$ ($\tau = 2$) labels the ground (excited) level, and $d^\dagger_{\tau,\boldsymbol{i}}$, $d_{\tau,\boldsymbol{i}}$ are the electron creation and annihilation operators in the $\boldsymbol{i}$th two-level system (TLS). Furthermore, L is the total number of TLSs, ω_i is the energy difference between the levels in the $\boldsymbol{i}$th TLS, ω_0 (ω) is the frequency of the incident (fluorescent) field, b_1 (b_2) annihilates a photon of the incident (fluorescent) field, g_{in} (g_{fl}) determines the coupling between the incident (fluorescent) field and the electron, Γ represents the phenomenological damping, u_e corresponds to the interaction between the excited electrons in the neighbouring TLS and $\tilde{n}^e_{\boldsymbol{i}}$ is the density of excited electrons in the $\boldsymbol{i}$th TLS.

Often the Dicke model is studied using ED. However, with the usual limitation met by ED for large systems, it is not possible to study Dicke systems with a large number L of TLS. Hence in our paper, we used the GKBA method for interacting electron-photon systems [17, 18]. As we observed before, GKBA scales quadratically with time. However, recently, a time-linear scaling method has been proposed for GKBA in the electronic case [19, 20]. Soon after that, the linear scaling formulation has been extended to interacting electron-boson systems [21, 22]. In what follows, we provide a brief survey of the method, following closely the original presentation in [21].

The bosonic GKBA is formulated in terms of the displacement $\varphi_{\mu,1} = \frac{1}{\sqrt{2}}(b^\dagger_\mu + b_\mu)$ and the momentum $\varphi_{\mu,2} = \frac{\mathrm{i}}{\sqrt{2}}(b^\dagger_\mu - b_\mu)$ of the boson mode μ. Similar to the electronic Green function, the photon counterparts are

$$D^<_{\bar{\mu}\bar{\nu}}(t,t') = D^>_{\bar{\nu}\bar{\mu}}(t',t) = -\mathrm{i}\left\langle \Delta\varphi_{\bar{\nu}}(t')\Delta\varphi_{\bar{\mu}}(t)\right\rangle, \tag{2.26}$$

where $\Delta\varphi_{\bar{\mu}}(t) = \varphi_{\bar{\mu}}(t) - \langle\varphi_{\bar{\mu}}(t)\rangle$, and $\bar{\mu}$ is a collective index $\bar{\mu} \equiv (\mu, \xi_\mu)$ with $\xi_\mu \in \{1, 2\}$. With the displacement and momentum operator, the boson Hamiltonian is $H_{bos} = \sum_{\bar{\mu}\bar{\nu}} \tilde{\Omega}_{\bar{\mu}\bar{\nu}}\,\varphi_{\bar{\mu}}\,\varphi_{\bar{\nu}}$, where $\tilde{\Omega}_{\bar{\mu}\bar{\nu}} = \frac{1}{2}\delta_{\mu\nu}\,\omega_\mu\,\delta_{\xi_\mu\xi_\nu}$. The time evolution of the correlator $D^{\lessgtr}$ has similar form as $G^{\lessgtr}$ (Eq. 2.20 and Eq. 2.21) with the boson self energy $\boldsymbol{\Sigma}_b$:

$$\left(\mathrm{i}\frac{d}{dt} - \boldsymbol{h}^b(t)\right)\boldsymbol{D}^<(t,t') = \boldsymbol{\mathcal{A}}\int_{-\infty}^{\infty} dt_1\Big(\boldsymbol{\Sigma}^R_b(t,t_1)\boldsymbol{D}^<(t_1,t') + \boldsymbol{\Sigma}^<_b(t,t_1)\boldsymbol{D}^A(t_1,t')\Big), \tag{2.27}$$

$$\boldsymbol{D}^>(t,t')\left(-\mathrm{i}\frac{\overleftarrow{d}}{dt'} - \boldsymbol{h}^b(t')\right) = \int_{-\infty}^{\infty} dt_1\Big(\boldsymbol{D}^R(t,t_1)\boldsymbol{\Sigma}^>_b(t_1,t') + \boldsymbol{D}^>(t,t_1)\boldsymbol{\Sigma}^A_b(t_1,t')\Big)\boldsymbol{\mathcal{A}}, \tag{2.28}$$

where $\boldsymbol{h}^b = \boldsymbol{\mathcal{A}}(\tilde{\boldsymbol{\Omega}} + \tilde{\boldsymbol{\Omega}}^T)$ is the effective bosonic Hamiltonian, and due to the commutation rules of bosons $\mathcal{A}_{\bar{\mu}\bar{\nu}} = -\delta_{\mu\nu}\begin{pmatrix} 0 & -\mathrm{i} \\ \mathrm{i} & 0 \end{pmatrix}_{\xi_\mu\xi_\nu}$.

To discuss the electron-boson coupling Hamiltonian H_{el-bos}, it is convenient to introduce the generalized indices $(g, \boldsymbol{j}) \to 2j-1$ and $(e, \boldsymbol{j}) \to 2j$. Accordingly, $H_{el-bos} = \sum_{\bar{\mu},ij} g_{\bar{\mu},ij}(t) d_i^\dagger d_j \varphi_{\bar{\mu}}$, where d_i destroys an electron at site i. Even in the presence of electron-boson coupling, the structure of the electron equation of motion will be the same as in Eq. 2.23, provided that we redefine the electron Hamiltonian. To this end, we consider $\tilde{h}^{HF}(t)$ instead of h^{HF} as

$$\tilde{h}^{HF}(t) = h(t) + V^{HF}(t) + \sum_{\bar{\mu}} g_{\bar{\mu},ij}(t) \big\langle \varphi_{\bar{\mu}}(t) \big\rangle. \tag{2.29}$$

Similar to Eq. 2.23, with the boson density matrix $\gamma^{\lessgtr}_{\bar{\mu}\bar{\nu}}(t) = \mathrm{i} D^{\lessgtr}_{\bar{\mu}\bar{\nu}}(t,t)$ and the boson collision integral $\boldsymbol{I}_b$, the boson equation of motion will be

$$\frac{d}{dt}\boldsymbol{\gamma}^<(t) + \mathrm{i}[\boldsymbol{h}^b(t), \boldsymbol{\gamma}^<(t)] = \boldsymbol{I}_b(t) + \boldsymbol{I}_b^\dagger(t). \tag{2.30}$$

The equation of motion is obtained using the boson GKBA (analogous to electron GKBA in Eq. 2.22),

$$\boldsymbol{D}^{\lessgtr}(t,t') = \boldsymbol{D}^R(t,t')\boldsymbol{\mathcal{A}}\boldsymbol{\gamma}^{\lessgtr}(t') - \boldsymbol{\gamma}^{\lessgtr}(t)\boldsymbol{\mathcal{A}}\boldsymbol{D}^A(t,t') \tag{2.31}$$

GKBA for the Dicke model

As mentioned before, we have studied the fluorescent spectra of the Dicke model (mentioned in Eq. 2.25) using the GKBA. In the study, we considered only the Hartree-Fock approximation for the electron Green function. Hence the only contribution to the electron collision integral $I_e(t)$ is from the electron-photon interaction , $I_{e,ij}(t) = \mathrm{i}\sum_{\bar{\mu},l} g_{\bar{\mu},il}(t) \mathcal{G}^b_{\bar{\mu},lj}(t)$, where $\mathcal{G}^b_{\bar{\mu},lj}(t) = \big\langle d_j^\dagger(t) d_l(t) \varphi_{\bar{\mu}}(t) \big\rangle_c$ [21], and the boson collision integral $I_{b,\bar{\mu}\bar{\nu}}(t) = -\mathrm{i}\sum_{mn} \bar{g}_{\bar{\mu},mn}(t) \mathcal{G}^b_{\bar{\nu},nm}(t)$, where $\bar{g}_{\bar{\mu},mn} = \sum_{\bar{\nu}} \mathcal{A}_{\bar{\mu}\bar{\nu}}\, g_{\bar{\nu},mn}$.

The high-order Green function $\mathcal{G}(t)$ includes integration over time; hence the GKBA method scales quadratically with time. As shown in [19, 20, 7] using the HF-GKBA as discussed above permits to perform the time evolution of the system in terms of time local coupled ordinary differential equations for G and $\mathcal{G}$. This is known as the 'G1-G2' scheme, where GKBA scales linearly with time, and this is the scheme we used in our study to make the calculations more efficient [21].

The coupled ordinary differential equations used in studying the Dicke model

are

$$\mathrm{i}\frac{d}{dt}\big\langle\varphi_{\bar\mu}(t)\big\rangle = \sum_{\bar\nu} h^b_{\bar\mu\bar\nu}(t)\big\langle\varphi_{\bar\nu}(t)\big\rangle + \sum_{ij}\bar g_{\bar\mu,ij}(t)\,\rho^<_{ji}(t), \tag{2.32}$$

$$\mathrm{i}\frac{d}{dt}\rho^<_{lj}(t) = [\tilde h^{HF}(t),\rho^<(t)]_{lj} + \bigg(\sum_{\bar\mu,i} g_{\bar\mu,li}(t)\mathcal{G}^b_{\bar\mu,ij}(t) - (l\leftrightarrow j)^*\bigg), \tag{2.33}$$

$$\mathrm{i}\frac{d}{dt}\gamma^<_{\bar\mu\bar\nu}(t) = [\boldsymbol{h}^b(t),\boldsymbol{\gamma}^<(t)]_{\bar\mu\bar\nu} + \bigg(\sum_{mn}\bar g_{\bar\mu,mn}(t)\mathcal{G}^b_{\bar\nu,nm}(t) - (\bar\mu\leftrightarrow\bar\nu)^*\bigg), \tag{2.34}$$

$$\mathrm{i}\frac{d}{dt}\mathcal{G}^b(t) = -\boldsymbol{\Phi}^b(t) + \boldsymbol{h}^b(t)\mathcal{G}^b(t) - \mathcal{G}^b(t)\tilde{\boldsymbol{h}}^e(t), \tag{2.35}$$

where $\boldsymbol{h}^e = \tilde h^{HF}\otimes I - I\otimes(\tilde h^{HF})^T$, $\boldsymbol{\Phi}^b(t) = \boldsymbol{\gamma}^>(t)\boldsymbol{g}(t)\boldsymbol{\rho}^<(t) - \boldsymbol{\gamma}^<(t)\boldsymbol{g}(t)\boldsymbol{\rho}^>(t)$ with $\boldsymbol{\rho}^< = \rho^<\otimes(\rho^>)^T$ and $\boldsymbol{\rho}^> = \rho^>\otimes(\rho^<)^T$.

For further details on the method, we refer the reader to the original presentation in [21, 22].

Chapter 3

Second Harmonic Generation

SHG is a nonlinear phenomenon, that was first observed in 1961 when passing laser beams through quartz crystals [23]. The use of laser beams was in fact necessary, since obtaining a well detectable signal from quartz required intense light sources. Nowadays, SHG is well characterized from both the theoretical and experimental point of view, and practically used in a wide range of applications. In many cases, SHG is theoretically described using nonlinear response theory, and often considering classical radiation fields. Nonetheless, there are aspects of SHG that remain at a good extent unexplored, for example the regime in which the average photon number is low and yet multi-photon fluctuations are relevant, where it is more appropriate to proceed with an equal footing quantum description of both matter and radiation. The aim of this chapter is to provide some basic notions of SHG, starting from a initial characterization in terms of the system's polarization and nonlinear susceptibilities [24, 25, 26, 27], and then motivate a description which is nonperturbative and fully quantum mechanical description for the radiation field, in the spirit of what is usually done for simple quantum models of nonlinear optics [28, 29, 30]. This last approach is the one which is used for the systems discussed in Papers I-III.

3.1 Polarization and harmonic generation

The light falling on a material could excite an electron to higher energy levels or lead to the separation of charges inducing polarization within the matter. The possibility of either situation depends on the frequency of the incident photon. In both cases, when matter undergoes relaxation, the absorbed energy will be

re-emitted with the emission of one or more photons.

The response of matter to an external electromagnetic field is described by the system's polarization $\boldsymbol{P}(\omega)$. If we expand $\boldsymbol{P}(\omega)$ in powers of the incident field, we have [24, 25, 26, 27]

$$\boldsymbol{P}(\omega) = \boldsymbol{P}^{(1)}(\omega) + \boldsymbol{P}^{(2)}(\omega) + \boldsymbol{P}^{(3)}(\omega) + ..., \tag{3.1}$$

where

$$\boldsymbol{P}^{(1)}(\omega) = \chi^{(1)}(\omega)\boldsymbol{E}(\omega) \tag{3.2}$$

$$\boldsymbol{P}^{(2)}(\omega) = \chi^{(2)}(\omega : \omega_1, \omega_2)\boldsymbol{E}(\omega_1)\boldsymbol{E}(\omega_2) \tag{3.3}$$

$$\boldsymbol{P}^{(3)}(\omega) = \chi^{(3)}(\omega : \omega_1, \omega_2, \omega_3)\boldsymbol{E}(\omega_1)\boldsymbol{E}(\omega_2)\boldsymbol{E}(\omega_3) \tag{3.4}$$

with $\omega = \omega_1 + \omega_2 + ... + \omega_n$ and

$$\chi^{(n)}(\omega : \omega_1, \omega_2, ..., \omega_n) = \int \chi^{(n)}(t_1, t_2, ..., t_n) e^{\mathrm{i}(\omega_1 t_1 + \omega_2 t_2 + ... + \omega_n t_n)} dt_1 dt_2 ... dt_n \tag{3.5}$$

In the equations, $\boldsymbol{E}(\omega_i)$ is the incident light field with the frequency ω_i. For an anisotropic system, the n-th order susceptibility $\chi^{(n)}$ is a tensor of rank $n+1$. For the two incident frequencies ω_a and ω_b, second order polarization could generate a sum, $\omega = \omega_a + \omega_b$ or a difference $\omega = \omega_a - \omega_b$ frequency. The sum frequency generated when $\omega_a = \omega_b$ doubles the incident field frequency, and this is known as second harmonic generation (SHG). Similarly, higher-order susceptibility terms will result in higher harmonic generation.

The relative magnitude of the susceptibilities of different orders can be estimated resorting to the Lorentz model of the atom, by considering the displacement of the electron cloud in response to the external electric field [31, 32], and the induced restoring force on the electron cloud. A restoring force that has a linear dependence on the displacement of the electron cloud is associated with a linear susceptibility behavior, whereas a nonlinear response/susceptibility corresponds to a restoring force which contains anharmonic contributions as well. Pursuing this line of argument, susceptibilities of consecutive order can be shown [31, 32, 26, 27] to be related as

$$\frac{|\chi^{(n)}(\omega)|}{|\chi^{(n-1)}(\omega)|} \approx \frac{1}{\mathcal{E}}, \tag{3.6}$$

where $\mathcal{E}$ is the modulus of average electric field strength inside an atom. With $E = |\boldsymbol{E}|$, the modulus of the incident light field, the polarization ratio is given by

$$\frac{P^{(n)}(\omega)}{P^{(n-1)}(\omega)} \approx \frac{E}{\mathcal{E}}. \tag{3.7}$$

For normal light, $E/\mathcal{E}$ is very small, and it is hard to observe nonlinear effects. However, with the intense light source with high E, nonlinear effects become more appreciable. Hence, the pioneering experimental observation of second harmonic generation happened [23] after the discovery of laser.

3.2 High harmonic generation

Producing high harmonic generation (HHG) with highly intense laser sources is of great [33, 34, 35] conceptual and practical significance, as also recognized in the motivations for the Nobel Prize awarded in 2023. For example, some important applications of HHG are the generation of attosecond pulses [36, 37, 38] and producing coherent extreme-ultraviolet or X-ray pulses [39, 40]. Theoretically, a popular and very often employed model to explain HHG in gases is the so-called three-step model [41, 42]. In this model, the electron is initially excited, then it accelerates in the presence of laser light, and finally recombines with the ion. The corresponding emitted radiation, related on the ionization potential and the kinetic energies of the accelerated electron, contributes to the HHG signal. For solids an analogous theoretical model can be adopted, in which electron motion in bands (intraband) [43] or electron transition between the bands (inter-band) [44, 45] is responsible for HHG. However, there are also alternative treatments available (for a review, see e.g. [25]).

3.3 Perturbation theory, Dressed states and Parity

As anticipated at the beginning of the chapter, in Papers I-III we consider situations where the average photon number is small but multi-photon fluctuations are relevant, using a nonperturbative and fully quantum mechanical treatment for the radiation field. The use of this level of description can be made plausible by considering two classical examples, namely the Mollow triplet and the Autler-Townes doublet.

To proceed, let us consider a one-electron, two-level atom, with $|g\rangle$ being the ground state and $|e\rangle$ being the excited state, in the presence of an incident field. The field has a frequency equal to the atom resonant frequency. Transitions are

possible between $|g, n\rangle$ and $|e, n-1\rangle$, which correspond to the excitation of the atom with the absorption of a photon and the de-excitation of the atom with the emission of a photon. This latter process will re-emit the absorbed photon with the same frequency as the incident photon. At resonance, the emission spectrum consists of three-peaks, and is known as 'Mollow spectrum' [46, 47]. In general, it is not possible to explain the Mollow triplet within a perturbative treatment. Perturbation theory can also be inadequate to describe another important effect, namely the Autler-Townes splitting [48, 49]. The latter is observed in a three-level atom when one of the transition levels is coupled to a third level via a strong auxiliary laser field.

A way to properly characterize the Mollow triplet and/or the Autler-Townes doublet is via the *dressed atom approach*, that we now briefly illustrate using a very popular model of quantum optics: the Jaynes-Cummings (JC) model [50]. The latter describes a model one-electron atom with two electronic levels (labeled $|g\rangle$ and $|e\rangle$, and with energies ϵ_g and ϵ_e, respectively) interacting with a single radiation mode. With the atom-photon coupling strength denoted by ζ, the JC Hamiltonian can be written as $H = H_0 + H_{int}$, where the interaction part (without rotating wave approximation, see below) is

$$H_{int} = \zeta(|g\rangle\langle e| + |e\rangle\langle g|)(a + a^\dagger), \tag{3.8}$$

and for the uncoupled Hamiltonian H_0 we have

$$H_0 = \epsilon_g|g\rangle\langle g| + \epsilon_e|e\rangle\langle e| + \omega_a a^\dagger a. \tag{3.9}$$

In Eqs. 3.8 and 3.9, $a^\dagger$ creates a photon of the cavity mode, the term $|g\rangle\langle e|a$ corresponds to the annihilation of a photon together with the atom de-excitation, and $|e\rangle\langle g|a^\dagger$ represents the creation of a photon during the atom excitation. When the photon frequency is close to the atom's resonance frequency, i.e., $\omega_a \approx \epsilon_e - \epsilon_g$, these terms in the Hamiltonian are usually neglected, according to what is known as rotating wave approximation (RWA) [50]. With the RWA, the Hamiltonian connects $|g, n\rangle$ only with $|e, n-1\rangle$. Hence the Hamiltonian will be block-diagonal, with the submatrix corresponding to $|e, n-1\rangle$ and $|g, n\rangle$ given by

$$H_n = \begin{bmatrix} \epsilon_e + (n-1)\omega_a & \zeta\sqrt{n} \\ \zeta\sqrt{n} & \epsilon_g + n\omega_a \end{bmatrix}. \tag{3.10}$$

The eigenvalues of H_n are [52]

$$E_{\pm,n} = \frac{(2n-1)\omega_a + \epsilon_e + \epsilon_g}{2} \pm \frac{1}{2}\sqrt{(\epsilon_e - \epsilon_g - \omega_a)^2 + 4\zeta^2 n}, \tag{3.11}$$

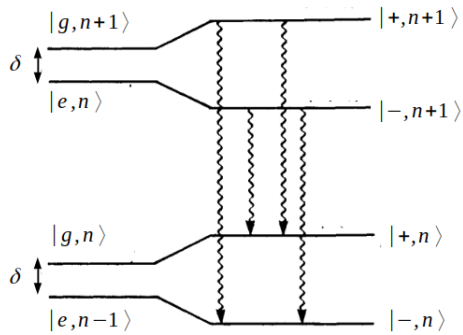

Figure 3.1: Energy spectrum of a two-level atom coupled to a photon field. In the figure the photon frequency is slightly larger than the resonance frequency of the atom, and hence the detuning $\delta = \omega_a - (\epsilon_e - \epsilon_g)$. The figure is adapted from [51].

with the corresponding (dressed) states given by

$$|+, n\rangle = \cos\,\theta_n|g, n\rangle + \sin\,\theta_n|e, n-1\rangle \tag{3.12}$$

$$|-, n\rangle = -\sin\,\theta_n|g, n\rangle + \cos\,\theta_n|e, n-1\rangle, \tag{3.13}$$

and

$$\tan(2\theta_n) = \frac{2\zeta\sqrt{n}}{\omega_a - (\epsilon_e - \epsilon_g)}.$$

At resonance, the dressed states $E_{+,n}$ and $E_{-,n}$ are separated by $2\zeta\sqrt{n}$. In a coherent state, for large $\langle n\rangle$ we have that $\sqrt{n} \approx \sqrt{\langle n\rangle}$ [51, 52, 53]. Hence among the four transitions between $E_{\pm,n}$ and $E_{\pm,n-1}$ (shown in Fig. 3.1), there are two degenerate transitions, and they are resonance transitions. The remaining two transitions form the side peaks of the Mollow spectrum.

The Autler-Townes doublet can also be explained within the dressed atom approach. A strong auxiliary laser field will lead to the dressing of the two atomic states. Hence a weak probe field will involve a transition between the third atomic level and the dressed states. Due to the transition between the atomic level and two close-dressed states, the doublet is observed in the emission spectra [54].

Photon-dressing effect can also have relevance for SHG. For example, in atoms, SHG is often described in terms of a three-level system model[53, 55]. Since SHG involves transitions among all the three states, for levels of definite parity, and in the perturbation regime, SHG will be forbidden. However, away from the perturbative regime, SHG can in fact even occur in a two level system, as a result of multi-photon dressing effects. We illustrate this by considering

again a photon field interacting with a two-level system. The total parity of the combined photon-field+TLS is a product of electron parity and photon field parity [56, 57, 53]:

$$\Pi = (n_g - n_e)e^{i\pi n_a}, \tag{3.14}$$

where n_g and n_e represent the density operator for an electron in the ground and the excited level respectively, and n_a is the photon density operator. The electron-photon Hamiltonian commutes with the total parity, $[H_0 + H_{int}, \Pi] = 0$. Even though the eigenstates of the full system will have a definite parity, the individual electron or photon subsystems will have indefinite parity. Thus, due to the dressing of the levels, conservation of electronic parity is not any more a constraint, and SHG is now allowed.

The situations briefly discussed here point to the importance of a non perturbative treatment of some matter-photon interaction phenomena and, specifically for our case, of SHG. Furthermore, aiming to investigate SHG in systems in optical cavities and at very weak fields (as done in Papers I-III, and where quantum fluctuations are important), a non perturbative and fully quantum treatment is in order.

3.4 Systems and photons in an optical cavity

The systems investigated in this thesis are assumed to be placed in a quantum optical cavity, and we here provide some general notions and definitions pertaining to this type of setup.

3.4.1 The SHG spectrum

Our general definition of the SHG spectrum, that we use in a full quantum description of the system and the photon fields, is

$$P(t,\omega) = \sum_{in} \sum_{m>0} |\langle inm|\mathcal{T}\left[e^{-i\int_0^t H(t')dt'}\right]|\psi(0)\rangle|^2, \tag{3.15}$$

where $|i\rangle$ represents the electron state, $|n\rangle$ represents the incident field number state, $|m\rangle$ represents the fluorescent field number state, $|\psi(0)\rangle$ is the initial state of the system, and H is the system Hamiltonian. It is worth emphasizing that H describes the material system, the quantized photon fields, and their mutual interaction, with many photon effects included in principle at all orders. Each of the papers I-III deals with different material systems. At same time, in all

cases, for the radiation part of H we consider two modes, respectively describing the cavity/incident and the fluorescent/SHG field.

3.4.2 Driving photons into the cavity

Our studies explored two ways of introducing photons into the cavity. One of the methods is driving photons into the cavity by the external laser field, and the other is by considering an initial coherent photon state.

In the first case, photons are introduced in the cavity by coupling the cavity photon mode to the external laser field. The initial state of the system is the ground state of the electron-photon coupled system (represented as $|\psi_0''\rangle$). The Hamiltonian representing the coupling between the external laser field and the cavity mode is

$$V_{drive} = g_d(b^\dagger + b)[f(t)\sin(\omega_0 t)], \tag{3.16}$$

where b annihilates an incident photon, g_d determines the laser field and the cavity mode coupling strength, ω_0 is the frequency of the laser field (same as the incident field frequency), and $f(t)$ provides an envelope to the external laser field. With the envelope function, it is possible to tune the time interval during which photons will be introduced into the cavity. In some cases, we used $f(t) = \theta(t_s - t)$, a step function vanishing after time t_s. However, in most cases we considered a rectangular envelope, $f(t) = [1 - \mathcal{F}_1(t)]\mathcal{F}_2(t)$ with the two Fermi functions $\mathcal{F}_i(t) = [\exp((t - t_i)/\tau) + 1]^{-1}$.

3.4.3 A coherent initial photon state

A coherent state is an eigenstate of the annihilation operator [58, 52], $b|\eta\rangle = \eta|\eta\rangle$. In terms of the photon number states, the coherent state follows the Poisson distribution,

$$|\eta\rangle = e^{-\frac{|\eta|^2}{2}} \sum_{k=0}^{\infty} \frac{\eta^k}{\sqrt{k!}} |k\rangle. \tag{3.17}$$

In our studies, we assumed in some cases that the initial state of the system is a product state of the material system and the photon fields. Specifically, the initial state is taken as $|\psi(0)\rangle = |\psi_0'\rangle = |Elc\rangle|\eta\rangle|0\rangle$, where $|Elc\rangle$ represents the initial state of the bare electron system and $|0\rangle$ corresponds to the vacuum state of the fluorescent field. This choice will be further discussed and motivated in section 4.3.

3.4.4 Cavity leakage with the classical bath

Photons inside the cavity will escape the cavity after some time. We account this cavity leakage in the spirit of the Caldeira-Leggett model (CLM) of dissipation [59], by coupling the photon mode to a bath of classical harmonic oscillators. The oscillators will remove the photons inside the cavity. The standard CLM is

$$H_{CLM} = \frac{p^2}{2m} + V(x) + \sum_k \left[\frac{{p_k}^2}{2m_k} + \frac{1}{2} m_k \omega_k^2 \left(x_k - \frac{c_k}{m_k \omega_k^2} x \right)^2 \right], \tag{3.18}$$

where p, m, x, and $V(x)$ represent the momentum, mass, position, and potential of the system (particle). Similarly, p_k, m_k, x_k, and ω_k corresponds to the bath oscillators. Note that p, x, p_k, x_k are in principle quantum mechanical operators. To describe leakage, we adapt Eq. 3.18 in order to couple the quantized cavity and/or fluorescent photon modes to the classical harmonic baths. For one photon mode of frequency $\tilde{\omega}$, described in second quantization, and treating p_k, x_k as classical variables, we arrive at:

$$\tilde{H}_{CLM} = \left(\tilde{\omega} + \sum_k \frac{C_k^2}{m_k \omega_k^2} \right) \tilde{b}^\dagger \tilde{b} + \sum_k \left(\frac{{p_k}^2}{2m_k} + \frac{1}{2} m_k \omega_k^2 x_k^2 \right) - \sum_k C_k x_k (\tilde{b}^\dagger + \tilde{b}) + \sum_k \frac{C_k^2}{m_k \omega_k^2} \left[\frac{(\tilde{b}^\dagger)^2 + \tilde{b}^2}{2} \right], \tag{3.19}$$

where $\tilde{b}$ destroys a photon of frequency $\tilde{\omega}$, and $C_k = c_k / \sqrt{2m\tilde{\omega}}$. In Eq. 3.19 we ignored the zero point energy.

We observed that with the Bogoliubov transformation $\begin{pmatrix} \tilde{b} \\ \tilde{b}^\dagger \end{pmatrix} = \begin{pmatrix} u & v \\ v & u \end{pmatrix} \begin{pmatrix} \mathcal{b} \\ \mathcal{b}^\dagger \end{pmatrix}$, it is possible to write Eq. 3.19 in a more compact form. After the Bogoliubov transformation, the redefined photon field is

$$\Omega_{\mathcal{b}} \mathcal{b}^\dagger \mathcal{b} = \left(\tilde{\omega} + \sum_k \frac{C_k^2}{m_k \omega_k^2} \right) \tilde{b}^\dagger \tilde{b} + \sum_k \frac{C_k^2}{m_k \omega_k^2} \left[\frac{(\tilde{b}^\dagger)^2 + \tilde{b}^2}{2} \right], \tag{3.20}$$

where $\Omega_{\mathcal{b}} = \sqrt{\tilde{\omega}^2 + 2m\tilde{\omega} \sum_k \frac{{C_k}^2}{m_k {\omega_k}^2}}$.

In both $\tilde{b}$ and $\mathcal{b}$ representation, the field position and momentum will remain the same. Hence $x = \frac{1}{\sqrt{2m\tilde{\omega}}} (\tilde{b}^\dagger + \tilde{b}) = \frac{1}{\sqrt{2m\Omega_{\mathcal{b}}}} (\mathcal{b}^\dagger + \mathcal{b})$ and $p = \mathrm{i} \sqrt{\frac{m\tilde{\omega}}{2}} (\tilde{b}^\dagger + \tilde{b}) =$

$\mathrm{i}\sqrt{\frac{m\Omega_\mathcal{b}}{2}}(\mathcal{b}^\dagger + \mathcal{b})$. Using these equations we can find that $u = (\sqrt{\frac{\tilde{\omega}}{\Omega_\mathcal{b}}} + \sqrt{\frac{\Omega_\mathcal{b}}{\tilde{\omega}}})/2$ and $v = (\sqrt{\frac{\tilde{\omega}}{\Omega_\mathcal{b}}} - \sqrt{\frac{\Omega_\mathcal{b}}{\tilde{\omega}}})/2$.

With the Bogoliubov transformation, Eq. 3.19 becomes

$$\tilde{H}_{CLM} = \Omega_\mathcal{b}\mathcal{b}^\dagger\mathcal{b} + \sum_k \left(\frac{{p_k}^2}{2m_k} + \frac{1}{2}m_k\omega_k^2 x_k^2 \right) - \sqrt{\frac{\tilde{\omega}}{\Omega_\mathcal{b}}} \sum_k C_k x_k (\mathcal{b}^\dagger + \mathcal{b}). \quad (3.21)$$

We used Eq. 3.19 to represent cavity leakage in papers I and II. However, in Paper III, we represent the cavity leakage with the transformed equation 3.21 for simplicity.

Chapter 4

Dimer in the optical cavity

As a first situation to study SHG in a cavity, we consider a model diatomic molecule (in the following referred to as 'dimer' for simplicity). This is rather a simple system for study, but it is interesting as it incorporates a great deal of physics and provides insight to more complicated system. We studied the resonance and SHG spectra of this system in Paper I. In our model, the dimer interacts with the two-photon fields, namely the cavity field and the emitted fluorescent field. The main intention of our study was to observe competition between the SHG and the molecule dissociation as shown in Fig. 4.1. The following section specifies the characteristics of the dimer model and its interaction with the cavity.

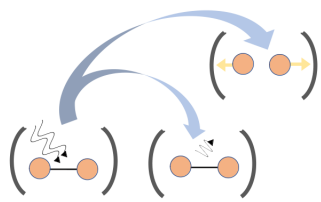

Figure 4.1: Schematic representation showing the competition between the SHG and the dimer dissociation.

4.1 Resonance frequency of the Dimer

Our model dimer in Paper I consists of atoms with one orbital, and two electrons of opposite spins. The electrons will interact when both the electrons are present on the same orbital/atom. As a novelty, along with the electrons, we consider

a quantum description also for the nuclear degrees of freedom. We observed in the study that, for the model dimer, the resonance frequency depends on the inter-nuclear distance, which is explained in detail in the following.

Considering for the moment the nuclei as classical, and assuming they are at rest at given positions (so that the nuclear momenta are zero), the dimer Hamiltonian, in the absence of the photon fields, reads

$$H_{mol} = \frac{C}{r_0^4} + \sum_{\sigma}(\epsilon_L n_{L\sigma} + \epsilon_R n_{R\sigma}) + \sum_{\sigma} V e^{-\xi r_0}(c^{\dagger}_{L\sigma} c_{R\sigma} + c^{\dagger}_{R\sigma} c_{L\sigma}) + U \sum_{i=L,R} n_{i\uparrow} n_{i\downarrow}, \tag{4.1}$$

where $c_{L\sigma}/c_{R\sigma}$ annihilates an electron of spin σ at site L/R (left/right), $n_{i\sigma} = c^{\dagger}_{i\sigma} c_{i\sigma}$ is a number operator, r_0 is the dimer inter-nuclear distance, ϵ_i is the onsite electron energy at site i, C determines the strength of inter-atomic repulsion, the effective hopping is $Ve^{-\xi r_0}$ with V representing the strength of hopping and ξ gives the dependence of the hopping on the inter-atomic distance. The repulsive and the attractive potentials together depicts a Morse-like potential.

The molecular electron energy levels determine the resonance frequency. The 2-particle site basis is $|L_\uparrow, L_\downarrow\rangle$, $|L_\uparrow, R_\downarrow\rangle$, $|R_\uparrow, L_\downarrow\rangle$ and $|R_\uparrow, R_\downarrow\rangle$, where $|L_\uparrow, L_\downarrow\rangle = c^{\dagger}_{L\uparrow} c^{\dagger}_{L\downarrow}|\text{vacuum}\rangle$. With the onsite energy $\epsilon_L = \epsilon_R = 0$, and the effective hopping $Ve^{-\xi r_0} = V'$, the Hamiltonian corresponding to the electron system is

$$H_e = \begin{pmatrix} U & V' & V' & 0 \\ V' & 0 & 0 & V' \\ V' & 0 & 0 & V' \\ 0 & V' & V' & U \end{pmatrix} \tag{4.2}$$

As next step, the symmetry-adapted 2-particle basis is constructed with the bonding (B) and the anti-bonding (A) states:

$$|B\rangle = \frac{1}{\sqrt{2}}(|L\rangle + |R\rangle), \quad |A\rangle = \frac{1}{\sqrt{2}}(|L\rangle - |R\rangle). \tag{4.3}$$

Hence the symmetry-adapted 2-particle basis is $|B_\uparrow, B_\downarrow\rangle$, $|A_\uparrow, A_\downarrow\rangle$, $|A_\uparrow, B_\downarrow\rangle$ and $|B_\uparrow, A_\downarrow\rangle$. Among the four basis vectors, $|B_\uparrow, B_\downarrow\rangle$ and $|A_\uparrow, A_\downarrow\rangle$ are even (E), $|A_\uparrow, B_\downarrow\rangle$ and $|B_\uparrow, A_\downarrow\rangle$ are odd (O) states. The Hamiltonian H_e with symmetry-adapted 2-particle basis is block diagonal,

$$H_e = \begin{pmatrix} H^E_{11} & H^E_{12} & 0 & 0 \\ H^E_{21} & H^E_{22} & 0 & 0 \\ 0 & 0 & H^O_{11} & H^O_{12} \\ 0 & 0 & H^O_{21} & H^O_{22} \end{pmatrix} \tag{4.4}$$

The matrix elements $H^E_{11} = 2V' + \frac{U}{2}$, $H^E_{22} = -2V' + \frac{U}{2}$ and other non-zero elements are $H^O_{11} = H^O_{22} = H^E_{12} = H^E_{21} = H^O_{12} = H^O_{21} = \frac{U}{2}$. The four eigenvalues of H_e are then

$$E_\pm = \frac{U \pm \sqrt{16V'^2 + U^2}}{2},$$
$$O_+ = U, \quad O_- = 0. \tag{4.5}$$

Here $E_\pm$ ($O_\pm$) represents the eigenvalues corresponding to even (odd) block.

The electron-photon interaction Hamiltonian is

$$H_{int} = \sum_\sigma g(c^\dagger_{A\sigma} c_{B\sigma} + c^\dagger_{B\sigma} c_{A\sigma})(a^\dagger + a). \tag{4.6}$$

Here g represents the electron-photon coupling strength, and a is a photon annihilation operator. Then the transition between E states or O states is forbidden because of parity. The dimer is considered to be in its ground state initially. We can observe that the ground state is an even state with the obtained eigenvalues. Hence parity allowed transitions are $E_- \leftrightarrow O_-$ and $E_- \leftrightarrow O_+$.

In our studies we observe fluorescence spectra. The fluorescent spectrum is obtained with the spin-preserving electron transitions. Hence involved eigenstates in the transitions must conserve the electron spin.

There are two electrons in the dimer; hence the total spin operator for the dimer is $\boldsymbol{S} = \boldsymbol{s}_1 + \boldsymbol{s}_2$. The dot product $\boldsymbol{S}^2 = \boldsymbol{S} \cdot \boldsymbol{S}$ is also expressed as

$$\boldsymbol{S}^2 = S_+ S_- + S_z^2 - S_z, \tag{4.7}$$

where $S_\pm = S_x \pm \mathrm{i} S_y$. In the one particle basis $S_z = \frac{1}{2}\sum_i (n_{i\uparrow} - n_{i\downarrow})$, $S_+ = \sum_i c^\dagger_{i\uparrow} c_{i\downarrow}$ and $S_- = \sum_i c^\dagger_{i\downarrow} c_{i\uparrow}$. Since the dimer electrons are of opposite spins, $S_z = 0$, and hence $\boldsymbol{S}^2 = S_+ S_-$. In the 2-particle site basis

$$\boldsymbol{S}^2 = \begin{pmatrix} 0 & 0 & 0 & 0 \\ 0 & 1 & -1 & 0 \\ 0 & -1 & 1 & 0 \\ 0 & 0 & 0 & 0 \end{pmatrix} \tag{4.8}$$

With the help of the above matrix, we can determine that both the even eigenstates are singlet states, the odd state $\frac{1}{2}(|B_\uparrow, A_\downarrow\rangle + |A_\uparrow, B_\downarrow\rangle)$ is also a singlet state, but the other odd state $\frac{1}{2}(|B_\uparrow, A_\downarrow\rangle - |A_\uparrow, B_\downarrow\rangle)$ is a triplet state.

For the fluorescence spectra, the transition is only possible between the singlet even state and the singlet odd state. The singlet odd state $\frac{1}{2}(|B_\uparrow, A_\downarrow\rangle + |A_\uparrow, B_\downarrow\rangle)$

corresponds to the eigenvalue $O_+ = U$. Since we assume the dimer to be in its ground state (with eigenvalue E_-), the resonance frequency will be

$$\Omega_R = \frac{U}{2} + \sqrt{4V'^2 + \left(\frac{U}{2}\right)^2}. \tag{4.9}$$

As we can observe in the expression, via V' the resonance frequency of the dimer is determined by the inter-nuclear distance. However, in our calculations, we consider a coupled electron-photon system. Coupling to the photon states will renormalize the bare electron states, leading to the dressed states as explained in section 3.3. The dressed states will mix the parity and allow transitions that are otherwise forbidden in the perturbation theory. Furthermore, restoring the quantum character of the nuclear degrees of freedom will have the result that quantum fluctuations will be associated with the average inter-nuclear distance.

4.2 Dimer interaction terms

In general, the Hamiltonian representing the Coulomb interaction between the electrons is

$$H_I = \frac{1}{2}\sum_{ijkl}\sum_{\sigma\sigma'} v_{ijkl} c^\dagger_{i\sigma} c^\dagger_{j\sigma'} c_{l\sigma'} c_{k\sigma} \tag{4.10}$$

where

$$v_{ijkl} = \int dxdy \phi^*_i(x)\phi^*_j(y) v(x,y)\phi_k(x)\phi_l(y). \tag{4.11}$$

Starting from Eq. 4.10 and Eq. 4.11, we wish to specialize the treatment to a diatomic system, and show how to arrive to the Hubbard type interaction used in our model molecule. To streamline the algebra, it is expedient to define an auxiliary problem, where there is an interaction $v_{ijkl} = F_{ij}G_{kl}$. Further, we define the operators $f^{\sigma\sigma'}_{ij} = \frac{c^\dagger_{i\sigma} c^\dagger_{j\sigma'} F_{ij}}{\sqrt{2}}$, and $g^{\sigma\sigma'}_{lk} = \frac{c_{l\sigma'} c_{k\sigma} G_{kl}}{\sqrt{2}}$. Hence the interaction Hamiltonian

$$H_I = \sum_{\sigma\sigma'}\sum_{ij} f^{\sigma\sigma'}_{ij} \sum_{kl} g^{\sigma\sigma'}_{lk}. \tag{4.12}$$

When the above Hamiltonian is reconsidered for the dimer, then all the site indices i, j, k and l will be restricted to the two dimer sites L and R. Then we can group the interaction Hamiltonian as follows,

$$H_I = H^1_I + H^2_I + H^3_I + H^4_I \tag{4.13}$$

with

$$H_I^1 = \sum_\sigma (f_{LL}^{\sigma\bar{\sigma}} + f_{RR}^{\sigma\bar{\sigma}})(g_{LL}^{\sigma\bar{\sigma}} + g_{RR}^{\sigma\bar{\sigma}}) \tag{4.14}$$

$$H_I^2 = \sum_\sigma (f_{LL}^{\sigma\bar{\sigma}} + f_{RR}^{\sigma\bar{\sigma}})(g_{LR}^{\sigma\bar{\sigma}} + g_{RL}^{\sigma\bar{\sigma}}) \tag{4.15}$$

$$H_I^3 = \sum_\sigma (f_{LR}^{\sigma\bar{\sigma}} + f_{RL}^{\sigma\bar{\sigma}})(g_{LL}^{\sigma\bar{\sigma}} + g_{RR}^{\sigma\bar{\sigma}}) \tag{4.16}$$

$$H_I^4 = \sum_{\sigma\sigma'} (f_{LR}^{\sigma\sigma'} + f_{RL}^{\sigma\sigma'})(g_{LR}^{\sigma\sigma'} + g_{RL}^{\sigma\sigma'}). \tag{4.17}$$

Here $\bar{\sigma}$ represents the opposite spin of σ, i.e. if $\sigma =\uparrow$ then $\bar{\sigma} =\downarrow$ and vice versa.

Now we use the definitions of the operators f and g,

$$\begin{aligned} H_I^1 = \frac{1}{2}\sum_\sigma (&v_{LLLL} c_{L\sigma}^\dagger c_{L\bar{\sigma}}^\dagger c_{L\bar{\sigma}} c_{L\sigma} + v_{LLRR} c_{L\sigma}^\dagger c_{L\bar{\sigma}}^\dagger c_{R\bar{\sigma}} c_{R\sigma} \\ &+ v_{RRLL} c_{R\sigma}^\dagger c_{R\bar{\sigma}}^\dagger c_{L\bar{\sigma}} c_{L\sigma} + v_{RRRR} c_{R\sigma}^\dagger c_{R\bar{\sigma}}^\dagger c_{R\bar{\sigma}} c_{R\sigma}). \end{aligned} \tag{4.18}$$

We can observe that, under the assumption $\phi_L(x) = \phi_R(x)$, $v_{LLRR} = v_{RRLL}$ and $v_{LLLL} = v_{RRRR}$ from Eq. 4.11. Hence,

$$H_I^1 = \frac{1}{2}\sum_\sigma v_{LLLL}(n_{L\sigma} n_{L\bar{\sigma}} + n_{R\sigma} n_{R\bar{\sigma}}) + \frac{1}{2}\sum_\sigma v_{LLRR}(c_{L\sigma}^\dagger c_{L\bar{\sigma}}^\dagger c_{R\bar{\sigma}} c_{R\sigma} + H.c.). \tag{4.19}$$

Further we assume that the dimer orbitals are real. Again from Eq. 4.11

$$v_{LLRL} = v_{LLLR} = v_{RRRL} = v_{RRLR} = v_{LRLL} = v_{LRRR} = v_{RLLL} = v_{RLRR}.$$

Thus the two interaction groups H_I^2 and H_I^3 becomes,

$$H_I^2 + H_I^3 = v_{LLLR}\sum_\sigma (n_{L\sigma} + n_{R\sigma})(c_{R\bar{\sigma}}^\dagger c_{L\bar{\sigma}} + H.c.). \tag{4.20}$$

Since the dimer contains two electrons of opposite spins, $n_{L\sigma} + n_{R\sigma} = 1$,

$$H_I^2 + H_I^3 = v_{LLLR}\sum_\sigma (c_{R\sigma}^\dagger c_{L\sigma} + H.c.). \tag{4.21}$$

The remaining interaction group becomes,

$$H_I^4 = -v_{RLLR}(S_R^+ S_L^- + S_R^- S_L^+) + v_{LRLR}\, n_L n_R - v_{RLLR}\sum_\sigma n_{L\sigma} n_{R\sigma}. \tag{4.22}$$

Here the spin ladder operators, $S_i^+ = c_{i\uparrow}^\dagger c_{i\downarrow}$, $S_i^- = c_{i\downarrow}^\dagger c_{i\uparrow}$ and the number operator $n_i = n_{i\uparrow} + n_{i\downarrow}$. The last term in the above equation can be re-expressed as

$$\sum_\sigma n_{L\sigma} n_{R\sigma} = 2\, S_L^z\, S_R^z + \frac{1}{2} n_L n_R, \tag{4.23}$$

where $S_i^z = \frac{1}{2}(n_{i\uparrow} - n_{i\downarrow})$. Using Eq. 4.23 in Eq. 4.22

$$\begin{aligned} H_I^4 &= -v_{RLLR}(S_R^+ S_L^- + S_R^- S_L^+) + v_{LRLR}\, n_L n_R - 2v_{RLLR} S_L^z\, S_R^z - \frac{1}{2} v_{RLLR}\, n_L n_R \\ &= -2v_{RLLR}\, \mathbf{S}_L \cdot \mathbf{S}_R + (v_{LRLR} - \frac{1}{2} v_{RLLR}) n_L n_R \end{aligned} \tag{4.24}$$

Combining all the groups, the complete interaction Hamiltonian for the dimer is,

$$\begin{aligned} H_I =& v_{LLLL}(n_{L\uparrow} n_{L\downarrow} + n_{R\uparrow} n_{R\downarrow}) + v_{LLRR}(c_{L\uparrow}^\dagger c_{L\downarrow}^\dagger c_{R\downarrow} c_{R\uparrow} + H.c.) \\ &+ v_{LLLR} \sum_\sigma (c_{R\sigma}^\dagger c_{L\sigma} + H.c.) + (v_{LRLR} - \frac{1}{2} v_{RLLR}) n_L n_R \\ &- 2v_{RLLR}\, \mathbf{S}_L \cdot \mathbf{S}_R \end{aligned} \tag{4.25}$$

We consider that the dimer orbitals are highly localized on the dimer sites L and R. Hence the overlap between the orbitals localized at L and R is very small. Thus the interaction integrals v_{LLLR}, v_{LLRR} and v_{RLLR} are negligible in comparison to v_{LLLL} and v_{LRLR} [60, 61].

Operators associated with v_{LRLR} are re-expressed as,

$$n_L n_R = n_{L\uparrow} n_{R\uparrow} + n_{L\uparrow} n_{R\downarrow} + n_{L\downarrow} n_{R\uparrow} + n_{L\downarrow} n_{R\downarrow} \tag{4.26}$$

Since we consider 2-particle site basis, $|L_\uparrow, L_\downarrow\rangle$, $|L_\uparrow, R_\downarrow\rangle$, $|R_\uparrow, L_\downarrow\rangle$ and $|R_\uparrow, R_\downarrow\rangle$, the first and the last terms of Eq. 4.26 are effectively 0. By using $n_{L\sigma} + n_{R\sigma} = 1$,

$$n_L n_R = 1 - n_{L\uparrow} n_{L\downarrow} - n_{R\uparrow} n_{R\downarrow} \tag{4.27}$$

Neglecting the constant term,

$$\begin{aligned} H_I &= (v_{LLLL} - v_{LRLR})(n_{L\uparrow} n_{L\downarrow} + n_{R\uparrow} n_{R\downarrow}) \\ &= U(n_{L\uparrow} n_{L\downarrow} + n_{R\uparrow} n_{R\downarrow}) \end{aligned} \tag{4.28}$$

represents the standard Hubbard interaction and we use this interaction in Paper I.

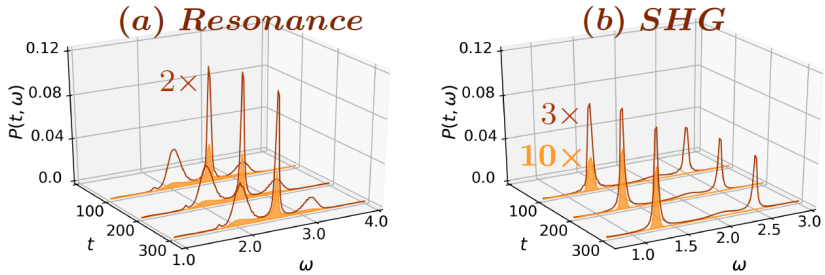

Figure 4.2: ***(a)*** Resonant spectra with $\omega_0 = \Omega_R$ and ***(b)*** SHG spectra for $\omega_0 = \Omega_R/2$, where Ω_R is the resonance frequency of the rigid molecule (in the calculations, $\Omega_R = 2.56$). Empty curves correspond to the coherent calculations using the initial state $|\psi_0'\rangle$ ($\eta^2 = 9$) and the filled curves represent the photon driving with the external laser field (with the initial state $|\psi_0''\rangle$). The drive is kept on until $\langle b^\dagger b\rangle \approx 9$, $t_1 = \frac{6\pi}{\omega_0}$, $t_2 = \frac{31\pi}{\omega_0}$ and $\tau = 2.0$, with $g_d = 0.229$ and 0.0996 in ***(a)*** and ***(b)*** respectively. Plots are scaled for visual clarity and the scaling factors are indicated in color. The Figure also appears in Paper I.

4.3 On the choice between coherent and driven states for cavity photon fields

We refer the reader to the actual papers for the results and the corresponding discussions. However, we mention here a general trend, namely how fluorescence is affected by the specific features of the incident field. This was first observed in Paper I, but the same behavior occurs for the systems of Paper II and III. Thus, we find it appropriate to discuss this point here using Paper I, since the trend in question motivates our choice of the incident field in all the papers.

In Paper I, introducing photons into the cavity by an initial coherent state, or via an external driving field, has a significant effect on the spectra. To illustrate this, in Fig. 4.2, we show the fluorescent spectra obtained with a coherent state and with a driving field for the steady state dimer. For the coherent state, we observe a Mollow like spectrum in the resonance case (Fig. 4.2 **(*a*)**, empty curves), whilst in the SHG case there is a generation of SHG signal (Fig. 4.2 **(*b*)**, empty curves). However, when we consider an external driving field, in the resonance case the intensity of the Mollow side peak gets reduced (Fig. 4.2 **(*a*)**, filled curves), and, in the case of second harmonics, the SHG peak gets quenched (Fig. 4.2 **(*a*)**, filled curves). In Paper I, we also considered a more detailed analysis with a two-level atom, and observed that one gets closer to the initial coherent state by increasing the speed of the driving (attained with an increased drive field coupling g_d, and a narrow envelope function $f(t)$).

Motivated by these considerations,in the papers we use a driving field at resonance and an initial coherent state for SHG.

Chapter 5

Optical lattices and cold atoms

Today ultracold atom physics represents a powerful and versatile platform to investigate many phenomena of condensed matter (and not only), offering an attractive alternative/complement to solid state systems because of the high flexibility that ultracold atom setups offer in e. g. tailoring the strength and shape of the one particle potential and particle-particle interactions. In this way, it is possible to address a great variety of different phenomena such as super-fluidity, super-solidity, Mott transitions, artificial gauge fields, to name a few [62, 63, 64]. This flexibility is to be traced back to the possibility of tuning Feshbach resonances to alter the interaction between ultracold atoms, and of accurately controlling counter propagating laser beams to provide a tunable periodic potential for the ultra-cold atoms [65, 66, 67, 68, 69].

5.1 Feshbach Resonances

Feshbach resonances, originally discussed by Feshbach in the context of nuclear reactions, have a key role in ultracold atom physics, since they permit to accurately tune the effective interaction among atoms [70, 62, 64]. This tunability is related to the manipulation of the hyperfine levels in an atom (due to the coupling between the electron and nuclear spin) and to the action/control of an external magnetic field. Feshbach resonances find application in both trapped-atom and optical-lattice setups (for example, they can be used to realize/stabilize (molecular) Bose-Einstein condensates). To qualitatively illustrate how the "resonance" aspect comes into play, one can consider a two-atom colliding system consisting of an open channel (associated with a low energy unbound state) and a closed

channel (associated with a bound molecular state). With an applied magnetic field one can vary the energy separation and the relative energetic ordering of the two channels and thus tune the interaction between the atoms. On a more formal ground, the possibility of tuning the interaction in a Feshbach resonance via applied magnetic field can be understood within the framework of scattering theory, where it is shown that, usually, in the dilute limit, the relevant/dominant scattering event occurs in the scattering s-channel, with the strength and sign of the interaction determined by the s-wave scattering length a_s. Providing a technical derivation of this statement is outside the scope of this thesis (also because, in Paper II, the focus is not on how the interactions among atoms are tuned), and we refer to the original literature (see e.g. [70]) for a thorough presentation of the subject.

Here we simply mention that, in the dilute limit, and in the presence of a magnetic field, a_s assumes the form

$$a_s \to a_s(B) = a_{op}\left(1 - \frac{\Delta}{B - B_0}\right), \tag{5.1}$$

where a_{op} is the background scattering length associated with the open channel, B is the applied magnetic field, B_0 is the critical magnetic field which brings degeneracy between the open, entrance channel energy and the closed, bound state channel energy, and Δ is the width of the resonance. Thus, by varying B one can tune the strength and the sign (via the channel-crossing at B_0) of $a_s(B)$ and control atom-atom interactions.

5.2 Optical lattice

Far from the resonance, the incident field will induce a dipole moment in the atom, $\boldsymbol{D} \propto \boldsymbol{E}$. And the atoms will feel potential energy $V(r) \propto E^2(r)$ in the presence of photon field [63]. Depending on whether the laser field is red detuned or blue detuned, atoms will be attracted or repelled respectively from the high-intensity region [64]. With two laser beams traveling in opposite directions, it is possible to form a periodic potential.

The optical lattice involves a periodic potential, a property associated with a crystal. Compared with the real crystals in the case of an atomic lattice, it is easy to tune the lattice parameters. The two waves traveling in the opposite direction form the standing wave pattern. The distance between the two optical lattice sites is hence half of the photon wavelength. But by combining laser lights with different angles and frequencies, it is possible to obtain optical lattices with

different patterns of periodic potentials [71, 72, 73] and thus vary the inter-atomic distances. Furthermore, by varying the intensity of the trapping laser field, it is possible to tune the tunneling of the atoms.

5.3 Phase transitions in an optical lattice

Since an optical lattice involves a periodic potential, there is a deep synergy between the two perspectives of i) using optical lattice to understand the Hubbard model and ii) using the Hubbard model to describe the properties of the atoms in an optical lattice. The bosonic or fermionic Hubbard model can be considered depending on whether the loaded atoms are fermions or bosons. In the following, as done in Paper II we only focus on boson case.

Mott insulator phase

Increasing the intensity of the laser field forming the optical lattice will decrease the hopping rate of the atom between the sites. The atoms are mostly trapped in the lattice sites with reduced hopping. With low hopping, the interaction between the atoms will be a dominant factor. The atoms in this situation will distribute themselves homogeneously among L_o lattice sites. At half filling this is a Mott insulator (MI) state represented by [74, 75]

$$|\Psi\rangle_{MI} \propto \prod_{i}^{L_o} \left(\alpha_i^\dagger\right)^{n_a} |0\rangle, \tag{5.2}$$

where α_i destroys an atom at site i and we assume n_a as number of atoms in each site.

Superfluid phase

When the interaction between the atoms is low, with the increased hopping, atoms are free to move around the entire lattice. Hence an atom will have its probability distributed over the entire lattice, and for bosons the superfluid state is well described by,

$$|\Psi\rangle_{SF} \propto \left(\sum_{i}^{L_0} \alpha_i^\dagger\right)^{N_a} |0\rangle, \tag{5.3}$$

which is a linear combination of different atomic occupations, and N_a is the total number of atoms loaded on the entire optical lattice. The phase diagram between these two regimes exhibits a complex pattern due to a co-existence line that divides the super fluid region from Mott insulator ones for different local occupancies. The phase diagram is usually displayed in $U - \mu$ plane (with U representing the interaction between the atoms and μ is the chemical potential). Many studies have analyzed the phase transition among MI and SF, and some recent studies include [76, 77, 78].

5.4 Model Hamiltonian

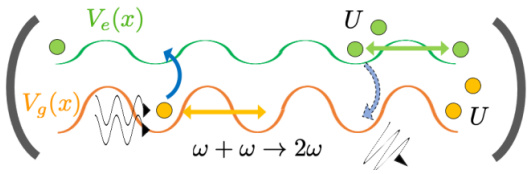

Figure 5.1: Schematic representation of the cold atoms in an optical lattice. The figure also appears in Paper II.

As shown in Fig. 5.1, we consider bosonic cold atoms in a one dimensional optical lattice interacting with a cavity and an emitted photon field. The cold atoms have two levels, ground level $|g\rangle$ and an excited level $|e\rangle$. The Hamiltonian for a two-level atom moving in such optical lattice is [75],

$$H_a^{(1)} = \frac{\hat{p}^2}{2m} + V_e(x)\,|e\rangle\langle e| + V_g(x)\,|g\rangle\langle g| + \omega_{eg}\,|e\rangle\langle e|\,, \tag{5.4}$$

where $V_{g/e}(x)$ represents the potential experienced by an atom in the ground/excited level in the optical lattice and ω_{eg} is the atomic excitation energy.

Along the same lines, the interaction Hamiltonian between the atom and the two photon fields is [75]

$$H_{a-p}^{(1)} = [\mathcal{G}_c(b_1 + b_1^\dagger) + \mathcal{G}_f(b_2 + b_2^\dagger)](|e\rangle\langle g| + |g\rangle\langle e|). \tag{5.5}$$

Here b_1 destroys an incident photon and b_2 destroys a fluorescent photon. The coupling strength of the cavity field and the fluorescent field with the atomic levels are determined by $\mathcal{G}_c$ and $\mathcal{G}_f$ respectively.

The bare photon fields are represented by the Hamiltonian

$$H_p = \omega_0 b_1^\dagger b_1 + \omega b_2^\dagger b_2, \tag{5.6}$$

an expression that is used also for the many-atom case. Next, we reconsider the above Hamiltonian terms in the many-atom case, using the second quantization formalism.

5.4.1 Atomic Hamiltonian

Considering the second quantization formalism, the independent particle part of the atomic Hamiltonian reads

$$H_a = \int dx \Psi_g^\dagger(x) \left[\frac{-\nabla^2}{2m} + V_g(x) \right] \Psi_g(x) + \int dx \Psi_e^\dagger(x) \left[\frac{-\nabla^2}{2m} + V_e(x) + \omega_{eg} \right] \Psi_e(x), \tag{5.7}$$

where $\Psi_i(x)$ is the atomic field operator representing the annihilation of an atom at position x. Delocalized Bloch states in a crystal can be expressed in terms of localized Wannier functions [79]. The same approach is adopted for the optical lattice, by expressing the field operators in terms Wannier functions. The latter are centered on the minimum potential points of the optical lattice[80, 81]. Since the ultra-cold atoms are kept at a temperature very close to absolute zero, the energy will not be sufficient to cause excitation to higher Wannier levels. Hence field operators will be represented only with the ground Wannier level.

$$\Psi_g(x) = \sum_i \alpha_i \Omega_g(x - x_i), \qquad \Psi_e(x) = \sum_i \beta_i \Omega_e(x - x_i) \tag{5.8}$$

where $\alpha_i(\beta_i)$ destroys an atom at ground(excited) state in site i.

In the Wannier basis, the atomic Hamiltonian in Eq. 5.7 will be rewritten as

$$\begin{aligned} H_a = \sum_{ij} \alpha_i^\dagger \alpha_j \int dx \Omega_g^*(x - x_i) \left[\frac{-\nabla^2}{2m} + V_g(x) \right] \Omega_g(x - x_j) \\ + \sum_{ij} \beta_i^\dagger \beta_j \int dx \Omega_e^\dagger(x - x_i) \left[\frac{-\nabla^2}{2m} + V_e(x) + \omega_{eg} \right] \Omega_e(x - x_j) \end{aligned} \tag{5.9}$$

Furthermore, as in tight binding treatments [82] for crystals, we make the assumption that the greatest contribution comes from the Wannier functions belonging to same site and the next nearest sites. Considering a homogeneous optical lattice with the same potential in each lattice site,

$$H_a = \sum_i \epsilon_g \alpha_i^\dagger \alpha_i + \sum_i \epsilon_e \beta_i^\dagger \beta_i + \sum_{\langle ij \rangle} t_g \alpha_i^\dagger \alpha_j + \sum_{\langle ij \rangle} t_e \beta_i^\dagger \beta_j \tag{5.10}$$

where $\epsilon_{g/e}$ and $t_{g/e}$ represents the onsite energy and the hopping of an atom in the ground/excited state. The energy $\epsilon_e - \epsilon_g$, which is now the resonance energy of the atom trapped in an optical lattice, it is different from the bare atomic transition ω_{eg}. The trapped atom resonance energy also includes the dressing of the cold atoms by the trapping photon field as in section 3.3.

5.4.2 Cold atoms and photon-atom interaction Hamiltonian

For highly localized Wannier functions, it is the case that

$$\int dx \Omega_g^*(x - x_i)\Omega_e(x - x_i) >> \int_{i \neq j} dx \Omega_g^*(x - x_i)\Omega_e(x - x_j). \tag{5.11}$$

Hence, the contribution from inter-site atomic excitations will be considerably smaller than the intrasite ones. With this assumption, the many-atom counterpart of Eq. 5.5 becomes

$$\begin{aligned} H_{a-p} = \sum_i \mathcal{G}_c \alpha_i^\dagger \beta_i \int dx \Omega_g^*(x - x_i)\Omega_e(x - x_i)(b_1^\dagger + b_1) + h.c. \\ + \sum_i \mathcal{G}_f \alpha_i^\dagger \beta_i \int dx \Omega_g^*(x - x_i)\Omega_e(x - x_i)(b_2^\dagger + b_2) + h.c. \end{aligned} \tag{5.12}$$

After performing the integrals and reabsorbing their value in the coupling constants,

$$H_{a-p} = g_c(b_1^\dagger + b_1) \sum_i (\alpha_i^\dagger \beta_i + h.c.) + g_f(b_2^\dagger + b_2) \sum_i (\alpha_i^\dagger \beta_i + h.c.) \tag{5.13}$$

5.4.3 Interaction term and final form of the total Hamiltonian

Expressing again the field operators in terms of Wannier functions, and using the same arguments given in the previous sections, one can argue that inter-site interaction terms will give a smaller contribution in comparison to onsite interaction terms. Hence, keeping only onsite interactions, the atom-atom interaction Hamiltonian can be written as

$$H_{a-a} = \frac{U_g}{2} \sum_i \alpha_i^\dagger \alpha_i^\dagger \alpha_i \alpha_i + \frac{U_e}{2} \sum_i \beta_i^\dagger \beta_i^\dagger \beta_i \beta_i + U_{eg} \sum_i \beta_i^\dagger \alpha_i^\dagger \alpha_i \beta_i \tag{5.14}$$

where $U_g(U_e)$ represents interactions among the atoms in the ground (excited) state, and U_{eg} describes the interaction between one atom in the ground state and the other in the excited state. We can rearrange H_{a-a} as follows:

$$H_{a-a} = \frac{U_g}{2}\sum_i n_i^g(n_i^g - 1) + \frac{U_e}{2}\sum_i n_i^e(n_i^e - 1) + U_{eg}\sum_i n_i^g n_i^e, \tag{5.15}$$

where n_i^g corresponds to the ground state atomic density at site i and similarly n_i^e corresponds to the excited atomic density. Finally, considering all the terms, the complete Hamiltonian for the cold boson atoms is

$$H = H_a + H_{a-a} + H_{a-p} + H_p, \tag{5.16}$$

or, more explicitly,

$$\begin{aligned} H = &\sum_i \epsilon_g \alpha_i^\dagger \alpha_i + \sum_i \epsilon_e \beta_i^\dagger \beta_i + \sum_{\langle ij\rangle} t_g \alpha_i^\dagger \alpha_j + \sum_{\langle ij\rangle} t_e \beta_i^\dagger \beta_j + \omega_0 b_1^\dagger b_1 + \omega b_2^\dagger b_2 \\ &+ \left[g_c(b_1^\dagger + b_1) + g_f(b_2^\dagger + b_2)\right]\sum_i(\alpha_i^\dagger \beta_i + h.c.) + U_g\sum_i n_i^g(n_i^g - 1) \\ &+ U_e\sum_i n_i^e(n_i^e - 1) + U_{eg}\sum_i n_i^g n_i^e. \end{aligned} \tag{5.17}$$

A similar Hamiltonian, but with only one photon field and within the RWA, can be found in [83].

5.5 A glance at Bose-Einstein condensates

When trapped boson atoms are brought to a very low temperature (close to absolute zero), all the atoms will occupy their ground state, and there will be a phase transition to a Bose-Einstein condensate (BEC) [84]. In Paper II, we also performed a preliminary study of SHG from a two-component BEC (2BEC) [85].

A fairly detailed derivation of the Hamiltonian for the 2BEC is provided in Paper II and not repeated here, also because it formally presents some similarities to the one discussed above for the two-level Bose Hubbard model [85]. As point worth mentioning, in the 2BEC case, the ground and the excited atom field operators $\Psi_g(x)$ and $\Psi_e(x)$ represent condensate modes [86], with the other higher excitations neglected. Specifically, $\Psi_g(x) = \tilde{\alpha}\phi_g(x)$ and $\Psi_e(x) = \tilde{\beta}\phi_e(x)$, where $\tilde{\alpha}$ annihilates an atom in the lowest condensate component and $\tilde{\beta}$ destroys an atom in the excited condensate component.

In Paper II, the 2BEC was considered to be inside an optical cavity, and interacting with both the cavity field and the fluorescent field. In terms of the condensate mode operators, the complete 2BEC+photon fields model Hamiltonian is

$$\begin{aligned} H_{BEC} =& \epsilon_g \tilde{\alpha}^\dagger \tilde{\alpha} + \epsilon_e \tilde{\beta}^\dagger \tilde{\beta} + \frac{U_g}{2N_a} \tilde{\alpha}^\dagger \tilde{\alpha}^\dagger \tilde{\alpha}\tilde{\alpha} + \frac{U_e}{2N_a} \tilde{\beta}^\dagger \tilde{\beta}^\dagger \tilde{\beta}\tilde{\beta} + \frac{U_{eg}}{N_a} \tilde{\beta}^\dagger \tilde{\alpha}^\dagger \tilde{\alpha}\tilde{\beta} \\ &+ \omega_0 b_i^\dagger b_i + \omega b_f^\dagger b_f + \Big[\frac{g_i}{\sqrt{N_a}} (b_i^\dagger + b_i) + \frac{g_f e^{-\Gamma t}}{\sqrt{N_a}} (b_f^\dagger + b_f) \Big] (\tilde{\alpha}^\dagger \tilde{\beta} + h.c.). \end{aligned} \quad (5.18)$$

In Eq. 5.18, the couplings and interactions are scaled with the number of atoms $\sqrt{N_a}$. The scaling is considered [87, 88] to contrast results for different number of particles and, in our case, to characterize in a consistent way the effect of cavity coupling and atom-atom interactions on the fluorescent spectra from the 2BEC.

Chapter 6

Conclusions and outlook

In this thesis, we broadly explained the process of SHG, described the numerical methods we used, and discussed the different systems examined in the papers. We hope this will provide the required background before reading the papers. This chapter is a brief summary of the papers and an outlook possible courses for future research.

As in the thesis title, our studies considered different systems inside an optical cavity, and we investigated the corresponding SHG spectra, to detect and characterize possible general trends. To this end we used rather simple theoretical models which, while offering a simplified perspective, are in many cases still effective in exhibiting qualitative trends.

In Paper I, we studied SHG from a dimer within an optical cavity. In this work, we mainly aimed to observe a competition between SHG and dimer dissociation. The resonance frequency in the system corresponds to the energy difference between the dimer's bonding and anti-bonding levels. Simultaneous absorption of two photons will excite the dimer to an anti-bonding state, promoting dimer dissociation. In our study, we observed that due to the slow nuclear motion of a heavy dimer, the dissociation will not occur; instead, a second harmonic signal will be generated. At the same time we observed the quenching of SHG in the case of a light dimer because dimer dissociation takes place. Also, photons will leave quickly in a bad cavity compared to a good cavity. In our paper, we demonstrated the role of cavity leakage by coupling the photon fields to a bath of (classical) oscillators. As expected, the cavity leakage reduced the spectrum intensity.

Paper II analyzed SHG from cold boson atoms in an optical lattice and from a

Bose-Einstein condensate. This study revealed a number of trends, specifically how the fluorescence varies when increasing the number of atoms, lattice sites and the strength of the atom-atom interaction. Also in this case, when including cavity leakage a decrease of the SHG response was observed.

For both Paper I and II, the methodology used was ED. However, ED becomes expensive or mostly impractical for larger systems. Hence, Paper III was devoted to exploring NEGF as an alternative approach to study SHG. As a test bed system we considered a very popular model of quantum optics namely the 'Dicke' model. Compared to the standard formulation we introduced disorder and the interaction in the model, to access less explored physics and make the model more interesting. In the study, we observed that disorder, interactions and cavity leakage lead to a decrease in SHG. In the range of parameters explored NEGF compared very favourably to ED benchmarks. Another aspect considered in Paper III, was the characterization of some scenarios with third harmonic generation. Similarly, one can extend the method to investigate the generation of higher harmonics.

As possible avenues for future work, it would be interesting to address multi-photon effects in a quantum description of SHG for more realistic systems. For example, one could consider more realistic molecules,or ultracold atoms with a space-dependent atom-cavity coupling. Alternatively, it would be of interest to consider model setups where one or more simple molecules are adsorbed on a surface. In a rather different direction, it could be interesting to address chaotic signatures in the fluorescent response, or the effect of photon entanglement on the generation of second and higher harmonics. Many of these possibilities,do escape the possibility of being treated within ED. However, as shown in this work, the great advantage of using NEGF is that one can tackle much larger and complex systems and situations than with ED, and thus hopefully many of the possible topics suggested here.

References

[1] S. Haroche and D. Kleppner, "Cavity Quantum Electrodynamics," *Physics Today*, vol. 42, pp. 24–30, 01 1989.

[2] T. J. Park and J. C. Light, "Unitary quantum time evolution by iterative Lanczos reduction," *The Journal of Chemical Physics*, vol. 85, pp. 5870–5876, 11 1986.

[3] C. Verdozzi, "Exact diagonalization studies of strongly correlated clusters," University of Milano-Bicocca, Italy: Lecture notes for the Doctorate Programme in Materials Science, 2005.

[4] A. Weiße and H. Fehske, "Exact diagonalization techniques," in *Computational Many-Particle Physics* (H. Fehske, R. Schneider, and A. Weiße, eds.), vol. 739.

[5] C. Lanczos, "An iteration method for the solution of the eigenvalue problem of linear differential and integral operators," *Journal of research of the National Bureau of Standards*, vol. 45, pp. 255–282, Oct 1950.

[6] E. Koch, "The lanczos method," in *The LDA+DMFT approach to strongly correlated materials* (E. Pavarini, E. Koch, D. Vollhardt, and A. Lichtenstein, eds.), Forschungszentrum Julich, Oct 2011.

[7] G. Stefanucci, "An essential introduction to negf methods for real-time simulations," in *Simulating Correlations with Computers Modeling and Simulation*, Forschungszentrum Jülich, 2021.

[8] G. Stefanucci and R. van Leeuwen, *Nonequilibrium Many-Body Theory of Quantum Systems: A Modern Introduction.* Cambridge University Press, 2013.

[9] M. Hopjan and C. Verdozzi, "Probing strongly correlated materials in non-equilibrium: Basic concepts and possible future trends in first principle

approaches," in *First Principles Approaches to Spectroscopic Properties of Complex Materials* (C. Di Valentin, S. Botti, and M. Cococcioni, eds.), pp. 347–384, Berlin, Heidelberg: Springer Berlin Heidelberg, 2014.

[10] K. Balzer and M. Bonitz, *Nonequilibrium Green's Functions Approach to Inhomogeneous Systems: Lecture Notes in Physics*. Springer Berlin, Heidelberg, 2012.

[11] P. C. Martin and J. Schwinger, "Theory of many-particle systems. i," *Phys. Rev.*, vol. 115, pp. 1342–1373, Sep 1959.

[12] L. V. Keldysh, "DIAGRAM TECHNIQUE FOR NONEQUILIBRIUM PROCESSES," *Soviet Phys. JETP*, vol. 20, pp. 1018–1026, Apr 1964.

[13] O. V. Konstantinov and V. I. Perel, "A DIAGRAM TECHNIQUE FOR EVALUATING TRANSPORT QUANTITIES," *Soviet physics JETP-USSR*, vol. 12, no. 1, pp. 142–149, 1961.

[14] P. Danielewicz, "Quantum theory of nonequilibrium processes, i," *Annals of Physics*, vol. 152, no. 2, pp. 239–304, 1984.

[15] P. Lipavský, V. Špička, and B. Velický, "Generalized kadanoff-baym ansatz for deriving quantum transport equations," *Phys. Rev. B*, vol. 34, pp. 6933–6942, Nov 1986.

[16] R. H. Dicke, "Coherence in spontaneous radiation processes," *Phys. Rev.*, vol. 93, pp. 99–110, Jan 1954.

[17] D. Karlsson, R. van Leeuwen, Y. Pavlyukh, E. Perfetto, and G. Stefanucci, "Fast green's function method for ultrafast electron-boson dynamics," *Phys. Rev. Lett.*, vol. 127, p. 036402, Jul 2021.

[18] N. Säkkinen, Y. Peng, H. Appel, and R. van Leeuwen, "Many-body Green's function theory for electron-phonon interactions: The Kadanoff-Baym approach to spectral properties of the Holstein dimer," *The Journal of Chemical Physics*, vol. 143, p. 234102, Dec 2015.

[19] N. Schlünzen, J.-P. Joost, and M. Bonitz, "Achieving the scaling limit for nonequilibrium green functions simulations," *Phys. Rev. Lett.*, vol. 124, p. 076601, Feb 2020.

[20] J.-P. Joost, N. Schlünzen, and M. Bonitz, "G1-G2 scheme: Dramatic acceleration of nonequilibrium green functions simulations within the hartree-fock generalized kadanoff-baym ansatz," *Phys. Rev. B*, vol. 101, p. 245101, Jun 2020.

[21] Y. Pavlyukh, E. Perfetto, D. Karlsson, R. van Leeuwen, and G. Stefanucci, "Time-linear scaling nonequilibrium green's function methods for real-time simulations of interacting electrons and bosons. I. formalism," *Phys. Rev. B*, vol. 105, p. 125134, Mar 2022.

[22] Y. Pavlyukh, E. Perfetto, and G. Stefanucci, "Interacting electrons and bosons in the doubly screened G$\widetilde{\text{W}}$ approximation: A time-linear scaling method for first-principles simulations," *Phys. Rev. B*, vol. 106, p. L201408, Nov 2022.

[23] P. A. Franken, A. E. Hill, C. W. Peters, and G. Weinreich, "GENERATION OF OPTICAL HARMONICS," *Phys. Rev. Lett.*, vol. 7, pp. 118–119, Aug 1961.

[24] A. Zheltikov, A. LHuillier, and F. Krausz, "Nonlinear optics," in *Springer Handbook of Lasers and Optics* (F. Träger, ed.), pp. 157–248, New York, NY: Springer New York, 2007.

[25] C. Attaccalite, D. Sangalli, and M. Grüning, "Non-linear response of solids and nanostructures: A real-time prospective," p. N°154, Mar. 2022. hal-03622296.

[26] G. S. He, *Nonlinear Optics and Photonics*. Oxford University Press, 10 2014.

[27] R. Boyd, *Nonlinear Optics*. Burlington: Academic Press, third edition ed., 2008.

[28] N. Bloembergen and Y. R. Shen, "Quantum-theoretical comparison of nonlinear susceptibilities in parametric media, lasers, and raman lasers," *Phys. Rev.*, vol. 133, pp. A37–A49, Jan 1964.

[29] D. F. Walls, "Quantum theory of nonlinear optical phenomena," *Journal of Physics A: General Physics*, vol. 4, p. 813, Nov 1971.

[30] N. Nayak and B. K. Mohanty, "Photon statistics of second-harmonic generation in a gaseous system," *Phys. Rev. A*, vol. 15, pp. 1173–1180, Mar 1977.

[31] M. P. Joshi, "Basics of nonlinear optics," in *Laser Physics and Technology* (P. K. Gupta and R. Khare, eds.), (New Delhi), pp. 27–64, Springer India, 2015.

[32] C. Garrett, "Nonlinear optics, anharmonic oscillators, and pyroelectricity," *IEEE Journal of Quantum Electronics*, vol. 4, pp. 70–84, 1968.

[33] M. Ferray, A. L'Huillier, X. F. Li, L. A. Lompre, G. Mainfray, and C. Manus, "Multiple-harmonic conversion of 1064 nm radiation in rare gases," *Journal of Physics B: Atomic, Molecular and Optical Physics*, vol. 21, p. L31, feb 1988.

[34] J. Eden, "High-order harmonic generation and other intense optical field–matter interactions: review of recent experimental and theoretical advances," *Progress in Quantum Electronics*, vol. 28, pp. 197–246, 2004.

[35] S. Zhong, Y. Liang, S. Wang, H. Teng, X. He, and Z. Wei, "High harmonic generation and application for photoemission spectroscopy in condensed matter," *Materials Futures*, vol. 1, p. 032201, Aug 2022.

[36] P. Antoine, A. L'Huillier, and M. Lewenstein, "Attosecond pulse trains using high–order harmonics," *Phys. Rev. Lett.*, vol. 77, pp. 1234–1237, Aug 1996.

[37] P. M. Paul, E. S. Toma, P. Breger, G. Mullot, F. Augé, P. Balcou, H. G. Muller, and P. Agostini, "Observation of a train of attosecond pulses from high harmonic generation," *Science*, vol. 292, pp. 1689–1692, 2001.

[38] M. Hentschel, R. Kienberger, C. Spielmann, G. A. Reider, N. Milosevic, T. Brabec, P. Corkum, U. Heinzmann, M. Drescher, and F. Krausz, "Attosecond metrology," *Nature*, vol. 414, pp. 509–513, Nov 2001.

[39] S. Han, "High-harmonic generation using a single dielectric nanostructure," *Photonics*, vol. 9, no. 6, 2022.

[40] R. L. Sandberg, A. Paul, D. A. Raymondson, S. Hädrich, D. M. Gaudiosi, J. Holtsnider, R. I. Tobey, O. Cohen, M. M. Murnane, H. C. Kapteyn, C. Song, J. Miao, Y. Liu, and F. Salmassi, "Lensless diffractive imaging using tabletop coherent high-harmonic soft-x-ray beams," *Phys. Rev. Lett.*, vol. 99, p. 098103, Aug 2007.

[41] P. B. Corkum, "Plasma perspective on strong field multiphoton ionization," *Phys. Rev. Lett.*, vol. 71, pp. 1994–1997, Sep 1993.

[42] R. Santra and A. Gordon, "Three-step model for high-harmonic generation in many-electron systems," *Phys. Rev. Lett.*, vol. 96, p. 073906, Feb 2006.

[43] M. Wu, S. Ghimire, D. A. Reis, K. J. Schafer, and M. B. Gaarde, "High-harmonic generation from bloch electrons in solids," *Phys. Rev. A*, vol. 91, p. 043839, Apr 2015.

[44] G. Vampa, C. R. McDonald, G. Orlando, P. B. Corkum, and T. Brabec, "Semiclassical analysis of high harmonic generation in bulk crystals," *Phys. Rev. B*, vol. 91, p. 064302, Feb 2015.

[45] L. Yue and M. B. Gaarde, "Introduction to theory of high-harmonic generation in solids: tutorial," *J. Opt. Soc. Am. B*, vol. 39, pp. 535–555, Feb 2022.

[46] B. R. Mollow, "Power spectrum of light scattered by two-level systems," *Phys. Rev.*, vol. 188, pp. 1969–1975, Dec 1969.

[47] R. E. Grove, F. Y. Wu, and S. Ezekiel, "Measurement of the spectrum of resonance fluorescence from a two-level atom in an intense monochromatic field," *Phys. Rev. A*, vol. 15, pp. 227–233, Jan 1977.

[48] J. Bai, J. Wang, S. Liu, J. He, and J. Wang, "Autler–townes doublet in single-photon rydberg spectra of cesium atomic vapor with a 319 nm uv laser," *Applied Physics B*, vol. 125, Feb 2019.

[49] S. M. Barnett and P. M. Radmore, *Methods in Theoretical Quantum Optics*. Oxford University Press, Nov 2002.

[50] W. P. Schleich, *Quantum Optics in Phase Space*. Berlin: John Wiley & Sons, Ltd, 2001.

[51] C. Cohen-Tannoudji, J. Dupont-Roc, and G. Grynberg, *Atom—Photon Interactions: Basic Process and Appilcations*. Weinheim: John Wiley & Sons, Ltd, 1998.

[52] G. Grynberg, A. Aspect, and C. Fabre, *Introduction to Quantum Optics: From the Semi-classical Approach to Quantized Light*. Cambridge University Press, 2010.

[53] E. Viñas Boström, A. D'Andrea, M. Cini, and C. Verdozzi, "Time-resolved multiphoton effects in the fluorescence spectra of two-level systems at rest and in motion," *Phys. Rev. A*, vol. 102, p. 013719, Jul 2020.

[54] C. N. Cohen-Tannoudji, *The Autler-Townes Effect Revisited*, pp. 109–123. New York, NY: Springer New York, 1996.

[55] K. Q. Lin, S. Bange, and J. M. Lupton, "Quantum interference in second-harmonic generation from monolayer WSe_2," *Nat. Phys.*, vol. 15, pp. 242–246, Mar 2019.

[56] S. He, C. Wang, Q.-H. Chen, X.-Z. Ren, T. Liu, and K.-L. Wang, "First-order corrections to the rotating-wave approximation in the Jaynes-Cummings model," *Phys. Rev. A*, vol. 86, p. 033837, Sep 2012.

[57] R. Birrittella, K. Cheng, and C. C. Gerry, "Photon-number parity oscillations in the resonant jaynes–cummings model," *Optics Communications*, vol. 354, pp. 286–290, 2015.

[58] C. Gerry and P. Knight, *Introductory Quantum Optics*. Cambridge University Press, 2004.

[59] A. O. Caldeira and A. J. Leggett, "Quantum tunnelling in a dissipative system," *Annals of physics*, vol. 149, no. 2, pp. 374–456, 1983.

[60] J. Hubbard, "Electron correlations in narrow energy bands," *Proceedings of the Royal Society of London. Series A, Mathematical and Physical Sciences*, vol. 276, no. 1365, pp. 238–257, 1963.

[61] A. P. Kądzielawa, A. Bielas, M. Acquarone, A. Biborski, M. M. Maśka, and J. Spałek, "H_2 and $(H_2)_2$ molecules with an ab initio optimization of wave functions in correlated state: electron–proton couplings and intermolecular microscopic parameters," *New Journal of Physics*, vol. 16, p. 123022, Dec 2014.

[62] C. Cohen-Tannoudji and D. Guéry-Odelin, *Advances in Atomic Physics: An Overview*. WORLD SCIENTIFIC, 2011.

[63] I. Bloch, "Ultracold quantum gases in optical lattices," *Nat. Phys.*, vol. 1, pp. 23–30, Oct 2005.

[64] M. Lewenstein, A. Sanpera, V. Ahufinger, B. Damski, A. Sen(De), and U. Sen, "Ultracold atomic gases in optical lattices: mimicking condensed matter physics and beyond," *Advances in Physics*, vol. 56, pp. 243–379, May 2007.

[65] C. Ospelkaus, S. Ospelkaus, L. Humbert, P. Ernst, K. Sengstock, and K. Bongs, "Ultracold Heteronuclear Molecules in a 3D Optical Lattice," *Phys. Rev. Lett.*, vol. 97, p. 120402, Sep 2006.

[66] S. Dürr, T. Volz, N. Syassen, D. M. Bauer, E. Hansis, and G. Rempe, "A Mott-like State of Molecules," *AIP Conference Proceedings*, vol. 869, pp. 278–283, Nov 2006.

[67] M. J. Bhaseen, A. O. Silver, M. Hohenadler, and B. D. Simons, "Feshbach Resonance in Optical Lattices and the Quantum Ising Model," *Phys. Rev. Lett.*, vol. 103, p. 265302, Dec 2009.

[68] O. Thomas, C. Lippe, T. Eichert, and H. Ott, "Experimental realization of a Rydberg optical Feshbach resonance in a quantum many-body system," *Nat. Commun.*, vol. 9, p. 2238, Jun 2018.

[69] C. J. Pethick and H. Smith, *Bose–Einstein Condensation in Dilute Gases*. Cambridge University Press, 2 ed., 2008.

[70] C. Chin, R. Grimm, P. Julienne, and E. Tiesinga, "Feshbach resonances in ultracold gases," *Rev. Mod. Phys.*, vol. 82, pp. 1225–1286, Apr 2010.

[71] L. Fallani, C. Fort, J. E. Lye, and M. Inguscio, "Bose-Einstein condensate in an optical lattice with tunable spacing: transport and static properties," *Opt. Express*, vol. 13, pp. 4303–4313, May 2005.

[72] L. Tarruell, D. Greif, T. Uehlinger, G. Jotzu, and T. Esslinger, "Creating, moving and merging dirac points with a fermi gas in a tunable honeycomb lattice," *Nature*, vol. 483, pp. 302–305, Mar 2012.

[73] G.-B. Jo, J. Guzman, C. K. Thomas, P. Hosur, A. Vishwanath, and D. M. Stamper-Kurn, "Ultracold Atoms in a Tunable Optical Kagome Lattice," *Phys. Rev. Lett.*, vol. 108, p. 045305, Jan 2012.

[74] M. Greiner, O. Mandel, T. Esslinge, T. W. Hänsch, and I. Bloch, "Quantum phase transition from a superfluid to a Mott insulator in a gas of ultracold atoms," *Nature*, vol. 415, pp. 39–44, Jan 2002.

[75] C. Maschler, I. B. Mekhov, and H. Ritsch, "Ultracold atoms in optical lattices generated by quantized light fields," *Eur. Phys. J. D*, vol. 46, pp. 545–560, Feb 2008.

[76] R. Jördens, N. Strohmaier, K. Günter, H. Moritz, and T. Esslinger, "A Mott insulator of fermionic atoms in an optical lattice," *Nature*, vol. 455, pp. 204–207, Sep 2008.

[77] R. Landig, L. Hruby, N. Dogra, M. Landini, R. Mottl, T. Donner, and T. Esslinger, "Quantum phases from competing short- and long-range interactions in an optical lattice," *Nature*, vol. 532, pp. 476–479, Apr 2016.

[78] D. Nagy, G. Kónya, P. Domokos, and G. Szirmai, "Quantum noise in a transversely-pumped-cavity Bose-Hubbard model," *Phys. Rev. A*, vol. 97, p. 063602, Jun 2018.

[79] W. Kohn, "Analytic Properties of Bloch Waves and Wannier Functions," *Phys. Rev.*, vol. 115, pp. 809–821, Aug 1959.

[80] M. Modugno and G. Pettini, "Maximally localized Wannier functions for ultracold atoms in one-dimensional double-well periodic potentials," *New Journal of Physics*, vol. 14, p. 055004, May 2012.

[81] J. Ibañez Azpiroz, A. Eiguren, A. Bergara, G. Pettini, and M. Modugno, "Tight-binding models for ultracold atoms in honeycomb optical lattices," *Phys. Rev. A*, vol. 87, p. 011602, Jan 2013.

[82] W. P. Lima, F. R. V. Araújo, D. R. da Costa, S. H. R. Sena, and J. M. Pereira, "Tight-binding Model in First and Second Quantization for Band Structure Calculations," *Braz. J. Phys.*, vol. 52, p. 42, Jan 2022.

[83] H. Zoubi and H. Ritsch, "Quantum phases of bosonic atoms with two levels coupled by a cavity field in an optical lattice," *Phys. Rev. A*, vol. 80, p. 053608, Nov 2009.

[84] A. J. Leggett, "Bose-Einstein condensation in the alkali gases: Some fundamental concepts," *Rev. Mod. Phys.*, vol. 73, pp. 307–356, Apr 2001.

[85] B. J. Dalton and S. Ghanbari, "Two mode theory of bose–einstein condensates: interferometry and the josephson model," *Journal of Modern Optics*, vol. 59, pp. 287–353, Feb 2012.

[86] L.-M. Kuang and L. Zhou, "Generation of atom-photon entangled states in atomic Bose-Einstein condensate via electromagnetically induced transparency," *Phys. Rev. A*, vol. 68, p. 043606, Oct 2003.

[87] E. Ghasemian and M. Tavassoly, "Dynamics of an atomic Bose–Einstein condensate interacting with nonlinear quantized field under the influence of Stark effect," *Physica A: Statistical Mechanics and its Applications*, vol. 562, p. 125323, 2021.

[88] D. Nagy, G. Kónya, G. Szirmai, and P. Domokos, "Dicke-Model Phase Transition in the Quantum Motion of a Bose-Einstein Condensate in an Optical Cavity," *Phys. Rev. Lett.*, vol. 104, p. 130401, Apr 2010.

Part II

Scientific publications

Printed by Media-Tryck, Lund 2024 NORDIC SWAN ECOLABEL 3041 0903

Lund University
Faculty of Science
Department of Physics

ISBN 978-91-8039-783-4